APPLIED SCIENCES AND ENGINEERING

Harnessing tissue-derived mitochondria-rich extracellular vesicles (Ti-mitoEVs) to boost mitochondrial biogenesis for regenerative medicine

Peng Lou[1]†, Xiyue Zhou[1]†, Yimeng Zhang[1], Yijing Xie[1], Yizhuo Wang[1], Chengshi Wang[2], Shuyun Liu[1], Meihua Wan[3], Yanrong Lu[1], Jingping Liu[1]*

Mitochondrial damage is a critical pathological factor in various forms of tissue injury, and specific therapies with high biosafety are desirable. Inspired by the natural role of extracellular vesicles (EVs) in regulating mitochondrial metabolism, we report that healthy tissue-derived mitochondria-rich EVs (Ti-mitoEVs) can boost mitochondrial biogenesis for regenerative medicine. Ti-mitoEVs that contain abundant functional mitochondria can be highly efficiently isolated from muscles via an optimized method. In vitro, Ti-mitoEV treatment increased mitochondrial biogenesis and reduced mitochondrial damage in recipient cells, and these effects occurred at least partly via mitochondrial genome transfer. In vivo, Ti-mitoEV treatment attenuated diverse types of tissue injury (e.g., muscle and kidney) by rescuing mitochondrial injury and its associated inflammation. As natural nanovesicles, the therapeutic potency of mitoEVs can be further improved by integrating them with other engineering methods. This study highlights the promising role of Ti-mitoEVs in boosting mitochondrial biogenesis, positioning them as potential therapies for treating various types of tissue injury characterized by mitochondrial damage.

INTRODUCTION

Mitochondria are multifaceted organelles engaged in regulating many cellular processes (e.g., energy metabolism, redox balance, and cell death) (*1*, *2*), and serve as central hubs to coordinate signaling cascades in controlling cell fate and tissue homeostasis (*3*). The critical roles of mitochondria in multicellular organisms render mitochondrial damage a key factor in various forms of tissue injury, such as heart (*4*), kidney (*3*), and skeletal muscle (*5*). For example, mitochondrial injury, as evidenced by elevated mitochondrial stress (mtROS), decreased mitochondrial biogenesis and energy depletion, has been extensively reported in both acute and chronic tissue injury (*6*, *7*). Thus, targeted restoration of mitochondrial function has been proposed as a therapeutic strategy for repairing diverse forms of tissue injury (*2*, *8*). Although some small chemical molecules, such as antioxidants (e.g., coenzyme Q_{10}) and Sirt1 activators (e.g., resveratrol), have been reported to mitigate some types of tissue injury by reducing mtROS production or improving mitochondrial biogenesis in animal models (*2*), their clinical translation remains limited by several limitations, such as a lack of tissue/organ specificity, limited bioavailability, short half-life, and side effects in vivo (*2*). Therefore, therapies with specific roles to boost mitochondrial metabolism with high biosafety are desirable for regenerative medicine.

Extracellular vesicles (EVs) are a group of heterogeneously secreted small vesicles (~30 to 1000 nm) that can affect the biofunctions of recipient cells by transporting various types of bioactive cargos (e.g., nucleic acids, proteins, and lipids) (*9*). To date, EV-based therapies have been shown to be promising means for tissue repair and regenerative medicine. In recent years, we and others have reported that diverse mitochondrial components, such as mitochondrial proteins, mitochondrial DNA (mtDNA), and fragmented or intact mitochondria, are enriched in certain EV subpopulations from cultured cells (*1*, *10*–*13*). These mitochondria-rich EVs (mitoEVs) can regulate multiple metabolic processes, such as mitochondrial biogenesis, oxidative phosphorylation (OXPHOS), and energy production, in recipient cells via direct mechanisms (e.g., transferring mitochondrial compositions) or indirect mechanisms (e.g., inducing mitochondrial mitophagy) (*14*, *15*). For example, mitochondria-containing EVs isolated from mouse or human brain endothelial cells (BECs) via differential ultracentrifugation (UC) have been reported to enhance mitochondrial function in injured BECs in vitro and reduce infarct sizes in mouse ischemic stroke in vivo (*16*–*19*). Notably, the released mitoEVs are considered natural regulators of mitochondrial functions, serving as an intrinsic mechanism for regulating cellular metabolism, the immune response, tissue homeostasis, and the injury repair process (*13*, *14*). Inspired by this endogenous phenomenon, we speculated that healthy tissue-derived mitoEVs (Ti-mitoEVs) might act as natural boosters of mitochondrial function to promote tissue injury repair. However, the optimized isolation methods and biological properties of Ti-mitoEVs, as well as their effects on tissue healing and action mechanisms, have not yet been explored.

Here, we report that Ti-mitoEVs are potential nanoboosters of mitochondrial biogenesis for regenerative medicine. In brief, we established an optimized method that enables high-efficiency, high-yield, and high-purity Ti-mitoEV production, and the isolated mitoEVs contained abundant functional mitochondrial components [e.g., whole mtDNA and electron transport chain (ETC) proteins]. In vitro, mitoEVs could increase mitochondrial biogenesis and reduce oxidative stress–induced mitochondrial injury in recipient cells through mitochondrial genome transfer. In vivo, mitoEVs significantly attenuated mitochondrial injury and its associated inflammatory response in acute or chronic forms of tissue injury. Multiomics analyses verified that the tissue protective effect of mitoEVs was dependent on restoring mitochondrial metabolism. This study indicates

[1]Department of General Surgery and NHC Key Laboratory of Transplant Engineering and Immunology, Frontiers Science Center for Disease-related Molecular Network, West China Hospital, Sichuan University, Chengdu 610041, China. [2]Department of Endocrinology and Metabolism, Center for Diabetes and Metabolism Research, West China Hospital, Sichuan University, Chengdu 610041, China. [3]West China Center of Excellence for Pancreatitis, Institute of Integrated Traditional Chinese and Western Medicine, West China Hospital, Sichuan University, Chengdu 610041, China.
*Corresponding author. Email: liujingping@scu.edu.cn
†These authors contributed equally to this work.

that Ti-mitoEV therapy can boost mitochondrial biogenesis and highlights that Ti-mitoEVs may serve as natural nanotherapeutics for treating tissue injury characterized by mitochondrial damage.

RESULTS AND DISCUSSION

High-efficiency isolation of endogenous Ti-mitoEVs from skeletal muscles

Previously, we and others reported that cultured cell [e.g., mesenchymal stromal cells (MSCs) and astrocytes]–derived EVs can play a protective role in tissue injury (e.g., acute kidney injury and hypoxic neurons) by reducing mitochondrial injury via the transfer of mitochondrial contents (*20*, *21*). However, the clinical translation of EVs derived from in vitro cultured cells is still limited by inefficient EV production and a lack of tissue-specific repair effects (*22*). Thus, endogenous mitoEVs directly isolated from healthy tissues might be a promising alternative to overcome these limitations. Skeletal muscle is one of the largest metabolic tissues of the body and contains abundant mitochondria (second to the heart, ~3 to 8% of the skeletal muscle volume) that produce adenosine 5′-triphosphate (ATP) to maintain its high metabolic requirements for locomotion (*23*, *24*). Emerging evidence indicates that certain mitochondrial contents of donor cells can be delivered to recipient cells via EVs (intercellular mitochondrial transfer), thereby regulating metabolic status and tissue homeostasis in physiological states (*14*). On the basis of these findings, we hypothesized that healthy skeletal muscle tissues contain substantial amounts of mitoEVs, which can participate in mediating mitochondrial metabolism and normal muscle functions. To this end, we first established an optimized method for the isolation of muscle Ti-mitoEVs, ensuring that such EVs more closely reflect their native state within the tissue microenvironment. An enzymatic digestion–based method was used to dissociate EVs from muscle tissues because it significantly shortened the EV production period and improved the EV yield (~8.73-fold increase in EV number per gram of muscle tissue) and EV purity (evidenced by a cleaner background under electron microscopy and a higher particle-protein ratio) compared to conventional tissue piece culture–based method (fig. S1, A to F).

Next, we aimed to separate the EV fractions and determine which EV fractions were enriched with mitochondrial contents. Previous studies have reported several methods for isolating mitochondria-derived EVs or mitoEVs, including density gradient UC (*11*, *25*) and differential UC (*12*, *15*). Although density gradient UC can obtain mitoEVs with the highest purity, this method is not ideal for therapeutic purposes because of its complicated operation procedure, time-consuming process, and low yield (*26*). As the most commonly used EV isolation method, modified differential UC might be more suitable for therapeutic mitoEV production because of its higher EV yield with acceptable EV purity. Many previous studies have used centrifugation at ~1000 to 2000*g* for removing cell debris and apoptotic bodies (*15*, *17*–*19*), and then used differential UC to categorize isolated EVs into large EVs (>2000 to 10,000*g*) and small EVs (>10,000 to 110,000*g*), and large EVs enriched with mitochondrial components are generally considered mitoEVs (*12*, *15*). However, given the wide range of centrifugation forces (g-force) for small EVs, large amounts of mitoEVs may also be included in this category. Thus, we further separated the small EVs into two fractions via different centrifugation forces (>10,000 to 50,000*g* and >50,000 to 110,000*g*) (fig. S2, A to F). The two fractions of small EVs presented different size distributions (fig. S2, B and D), and the >10,000 to 50,000*g* fraction also contained abundant mitochondrial proteins and mtDNA. The levels of certain mitochondrial proteins [e.g., cytochrome c oxidase subunit 4 (COXIV) and voltage-dependent anion channel (VDAC)] in this small EV subfraction were similar to those in large EVs (fig. S2, G to I), suggesting the coexistence of many mitoEVs in the previously defined small EV category.

To precisely isolate mitoEVs from muscle tissues, we further set up a denser centrifugal gradient including five fractions with different centrifugation forces: low (>2000 to 10,000*g*, 10K), low-medium (>10,000 to 20,000*g*, 20K), medium (>20,000 to 30,000*g*, 30K), medium-high (>30,000 to 50,000*g*, 50K), or high (>50,000 to 110,000*g*, 110K) (Fig. 1A). Transmission electron microscopy (TEM) revealed that EV fractions pelleted at 10K, 20K, or 30K contained numerous heterogeneous EV subpopulations with wide size distributions (~30 to 467 nm) (Fig. 1, B to D), whereas EV fractions pelleted at 50K or 110K had a more uniform size distribution and were smaller (~30 to 189 nm) than those pelleted at 10K, 20K, or 30K (Fig. 1, B to D). In each fraction, the EV yield calculated from the protein amounts did not positively correlate with the EV yield calculated from the particle numbers (Fig. 1E), suggesting distinct protein amounts or compositions at the single EV level. The protein amount per EV pelleted at low speed (10K) was higher than that at 20K, 30K, 50K, or 110K (Fig. 1F), which again indicated the heterogeneity of EV subpopulations. Compared with those at 50K to 110K, the muscle EV fractions at 10K to 30K contained significantly higher levels of mitochondrial contents, including mtDNA and mitochondrial proteins [e.g., COXIV, ATP synthase F1 subunit alpha (ATP5a), VDAC, translocase of outer mitochondrial membrane 20 (TOM20), and pyruvate dehydrogenase (lipoamide) beta (PDHB)] (Fig. 1, G and H, and fig. S3). On the basis of these results, we termed the EV fractions between 2000 and 30,000*g* as mitoEVs because of their enriched mitochondrial contents, and named the other EV fractions (30,000 to 110,000*g*) as non-mitoEVs. Compared with conventional large EVs, our mitoEVs presented a significantly higher EV yield (~4.7-fold greater in EV particles and ~3.1-fold greater in EV protein) and comparable levels of mitochondrial proteins (e.g., COXIV, ATP5a, VDAC, TOM20, and PDHB) or mtDNA (Fig. 1, I to L), indicating their potential for therapeutic applications.

Furthermore, high-resolution flow cytometry analysis was used to verify that the mitoEV preparations mainly comprise structurally intact EVs rather than protein or other particle contaminants, as previously reported (*27*, *28*). Carboxyfluorescein diacetate succinimidyl ester (CFSE) is a membrane-permeable dye that can passively diffuse into EVs. Although CFSE itself has no fluorescence, it is converted into a fluorescent form by active esterases within EVs, thus indicating the existence of an intact EV membrane (*27*). CFSE staining does not disrupt EV structure, induce EV aggregation, or generate artificial nanoparticles (*27*, *28*). As shown in fig. S4 (A and B), there was a significant reduction in $CFSE^+$ mitoEV events after Triton X-100 treatment, which is consistent with EV lysis induced by detergent-mediated membrane disruption and indicates that our EV preparations consisted mainly of intact vesicles.

Muscle Ti-mitoEVs carry abundant functional mitochondrial components

EVs can affect the phenotype and function of target cells by transferring various bioactive cargos (*22*, *29*). Owing to their heterogeneity, different EV subpopulations may have varied sizes and/or compositions,

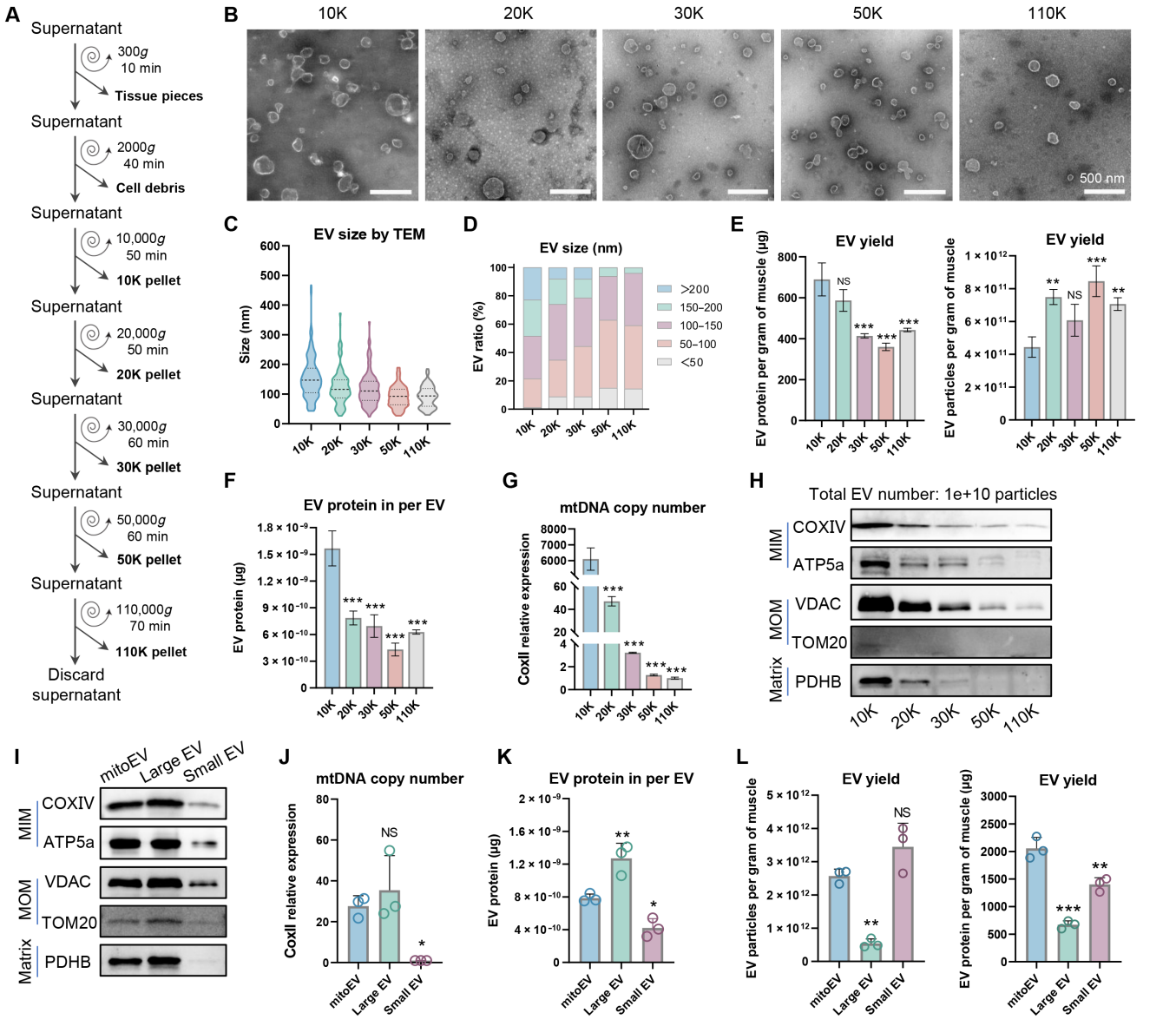

Fig. 1. Isolation and characterization of tissue-derived mitoEVs. (**A**) Schematic diagram of the isolation of different EV fractions. (**B**) Representative TEM images of different EV fractions (scale bar = 500 nm). (**C** and **D**) EV size distributions determined on the basis of TEM images. (**E**) EV yield of different EV fractions ($n = 3$). (**F**) EV protein amounts at the single EV level ($n = 3$). (**G**) mtDNA copy number of different EV fractions ($n = 3$). (**H**) Mitochondrial protein content of different EV fractions. (**I**) Comparison of the mitochondrial protein content of mitoEVs, large EVs, and small EVs. (**J**) Comparison of the mtDNA copy numbers of mitoEVs, large EVs, and small EVs ($n = 3$). (**K**) EV protein amounts at the single EV level in mitoEVs, large EVs, and small EVs ($n = 3$). (**L**) EV yield of mitoEVs, large EVs, and small EVs ($n = 3$). $^*P < 0.05$, $^{**}P < 0.01$, $^{***}P < 0.001$, and NS = not significant.

along with diverse biofunctions. Thus, we compared the characteristics of mitoEVs and non-mitoEVs isolated from the same muscle tissues (Fig. 2, A to C, and fig. S5A). As shown in Fig. 2, B and C, mitoEVs had a wider size distribution with higher populations of larger EVs (>200 nm) compared to non-mitoEVs. The protein amount per EV was also higher (~1.65-fold) in mitoEVs than in non-mitoEVs (Fig. 2D), which may be due to the presence of abundant mitochondrial contents in mitoEVs. To evaluate the global differences in EV composition, the protein profiles of mitoEVs and non-mitoEVs were analyzed via liquid chromatography–tandem mass spectrometry (MS)–based proteomics. A principal components analysis (PCA) scatter plot clearly revealed distinct protein expression patterns between the mitoEVs and the non-mitoEVs (Fig. 2E). A total of 673 differentially expressed proteins (DEPs) were identified, of which 536 DEPs were highly expressed in mitoEVs and 137 DEPs were highly expressed in non-mitoEVs (Fig. 2F). Further gene ontology (GO) enrichment analysis revealed that the up-regulated DEPs of the mitoEVs were associated mainly with the mitochondria (mitochondrial membrane and mitochondrial matrix) and organelle membrane (Fig. 2G), and they might be involved in mitochondria-related

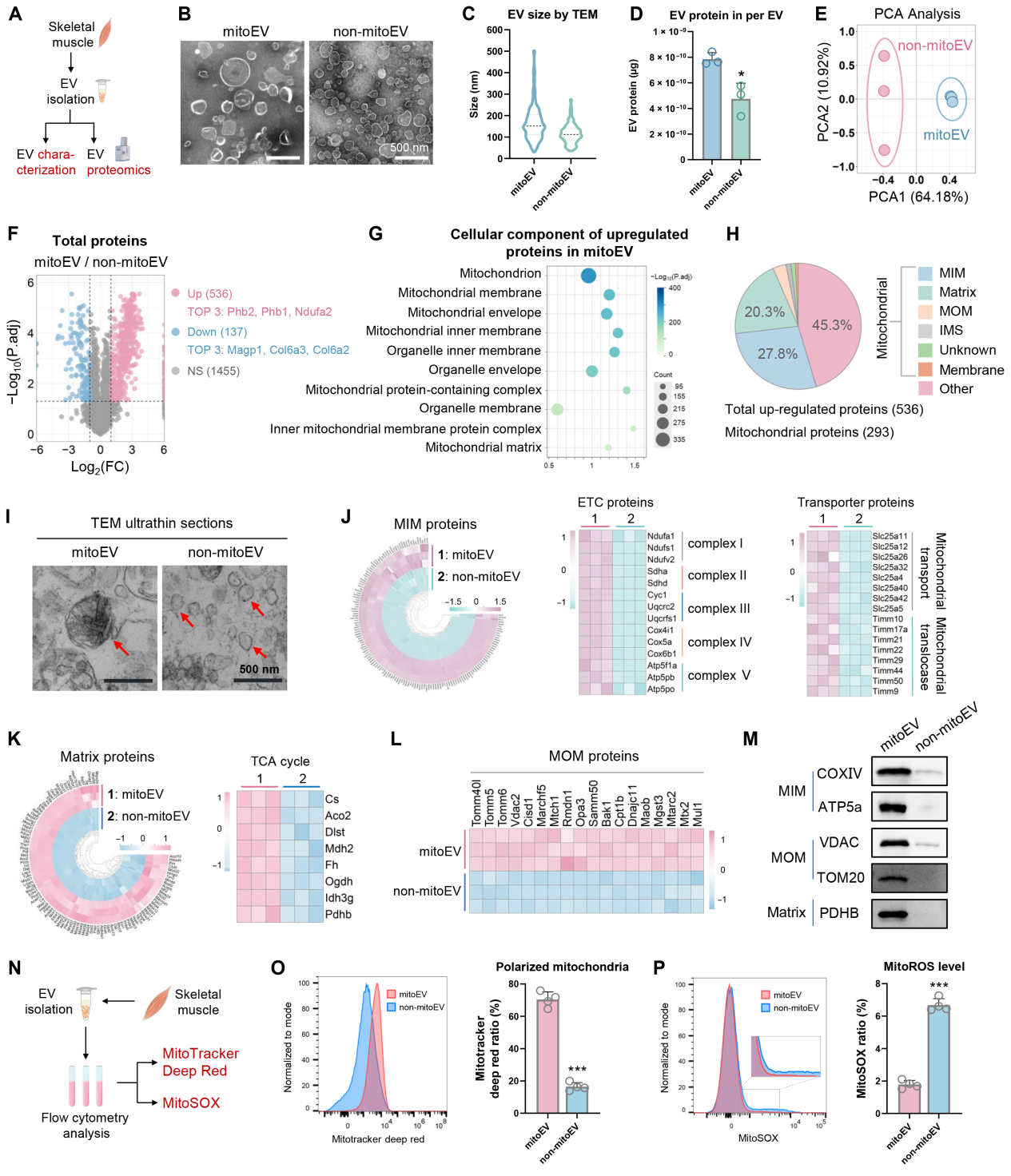

Fig. 2. Evaluating the compositional signatures of mitoEVs and non-mitoEVs. (**A**) Schematic diagram of the EV component investigation. (**B**) Representative TEM images of mitoEVs and non-mitoEVs (scale bar = 500 nm). (**C**) EV size distribution determined based on TEM images. (**D**) EV protein amounts at the single EV level ($n = 3$). (**E**) PCA score plot representing discrepancies between mitoEVs and non-mitoEVs ($n = 3$). (**F**) Volcano plots showing the number of DEPs between mitoEVs and non-mitoEVs (FC > 2 and *P*-adjusted <0.05). (**G**) GO cellular component analysis of the up-regulated DEPs of mitoEVs. (**H**) The proportion of mitochondrial proteins among the DEPs. (**I**) Representative TEM ultrathin section images of mitoEVs and non-mitoEVs (scale bar = 500 nm). (**J** to **L**) Heatmap of the mitochondrial protein DEPs between mitoEVs and non-mitoEVs. (**M**) Comparison of the mitochondrial protein content between mitoEVs and non-mitoEVs. (**N**) Schematic diagram of mitoEV functional component investigation. (**O**) MMP detection of mitoEVs and non-mitoEVs using high-resolution flow cytometry ($n = 4$). (**P**) Mitochondrial ROS levels in mitoEVs and non-mitoEVs determined using high-resolution flow cytometry ($n = 4$). *$P < 0.05$, **$P < 0.01$, ***$P < 0.001$, and NS = not significant.

biological processes, such as cellular respiration, ATP synthesis, mitochondrial transport, and the tricarboxylic acid cycle (fig. S5, B and C). The number of mitochondrial proteins accounted for more than half (~54.7%) of the up-regulated proteins in the mitoEVs (Fig. 2H). In contrast, the proteins enriched in non-mitoEVs primarily originated from muscular cell functional components (e.g., myosin complex, myofibril, and myosin filament) and the cytoskeleton, and they were enriched in pathways related to muscle contraction and muscle system processes (fig. S5, D to F). These results indicate distinct composition signatures between mitoEVs and non-mitoEVs, which may contribute to their diverse biological roles in regulating muscle tissue homeostasis and repair.

Further analysis revealed that the majority of proteins (~75%) detected in mitoEVs, in particular mitochondrial proteins (~76.5%), overlapped with those cataloged in the Vesiclepedia database (fig. S6, A to E). The remaining proteins were enriched primarily in pathways related to muscle development/metabolism and mitochondrial metabolism (fig. S6, B and D). Notably, mitoEVs contain almost all the mitochondrial inner membrane (MIM) proteins reported in the Vesiclepedia (~81.4%) and Exocarta (~95.2%) databases, as well as most of the mitochondrial outer membrane (MOM) proteins and matrix proteins documented in these databases (fig. S6E). These results indicate that the proteins carried by mitoEVs broadly overlap with the established EV protein databases, despite the presence of several additional unique proteins. The possible reason is that the existing EV databases predominantly catalog proteins from cultured cell–derived EVs, whereas mitoEVs are from more complicated tissue microenvironments. In addition, methodological variations in EV isolation and/or proteomic profiling across different studies may contribute to incomplete overlap, as exemplified by differences between the Vesiclepedia and Exocarta databases themselves.

Next, we assessed the integrity and functionality of the mitochondrial contents in mitoEVs. TEM ultrathin sections revealed the existence of a mitochondrial structure in mitoEVs but not in non-mitoEVs (Fig. 2I), and this effect might be due to their different sorting routes or surface area–to–volume ratios. Through proteomics analysis, a total of 365 mitochondrial proteins were identified in mitoEVs or non-mitoEVs, of which 293 mitochondrial proteins were expressed at higher levels in mitoEVs than in non-mitoEVs (fig. S7). The mitochondrion mainly consists of the MIM, the MOM, and the mitochondrial matrix, in which the MIM and matrix are the main compartments of mitochondrial metabolism (*30*). As shown in Fig. 2 (J to L), mitoEVs were enriched with numerous MIM proteins, such as ETC proteins (e.g., ETC complexes I to V) and transporters (e.g., Slc25a5, Timm10, and Timm21), mitochondrial matrix proteins (e.g., Cs, Pdhb, and Aco2), and MOM proteins (e.g., Tomm40, Vdac2, and Cpt1b). Further immunoblotting verified that mitoEVs had higher levels of MIM (e.g., COXIV and ATP5a), MOM (e.g., VDAC and TOM20), and matrix (e.g., PDHB) proteins compared to non-mitoEVs (Fig. 2M and fig. S8).

In addition to proteins, mitochondria have their own genome [16.3-kb circular double-stranded DNA (dsDNA)], which encodes 13 critical ETC proteins and is essential for mitochondrial biogenesis, OXPHOS and energy generation (*31*). Consistent with the protein results, the mtDNA contents carried by mitoEVs were also significantly higher (~663.6-fold) than those carried by non-mitoEVs (Fig. 3A). We next determined whether the mitoEVs carried intact mtDNA, since some reports have indicated that EVs might contain fragmented mtDNA contents (*32*). Long-range polymerase chain reaction (PCR) was performed with two reported amplicons covering the entire mtDNA genome as previously reported (Fig. 3B) (*33*). The results revealed that mitoEVs contained mtDNA with a complete 16.3-kb circular dsDNA, whereas non-mitoEVs carried many fragmented mtDNAs (Fig. 3C), indicating the existence of the whole mitochondrial genome in mitoEVs.

Given that mitoEVs contain almost all types of mitochondrial proteins and whole mtDNA, we sought to assess whether the mitochondrial components of mitoEVs are functional (Fig. 2N). The mitochondrial membrane potential (MMP) is a hallmark of mitochondrial activity and can be used to assess functional mitochondrial aspects, such as the proton motive force and OXPHOS (*34*). The isolated mitoEVs or non-mitoEVs were stained with MitoTracker Deep Red Probes (MDR; a specific dye indicating polarized mitochondria), and mitoEVs presented higher levels of polarized mitochondria than non-mitoEVs did (Fig. 2O), indicating that the mitochondria in mitoEVs were at least partly functional. Similarly, it has been reported that EVs derived from mitochondria have a membrane potential with ATP generation ability (*35*). In addition, functional mitochondria can generate superoxide (O_2^-) as a bypass product during OXPHOS, whereas excessive superoxide production indicates mitochondrial injury. Both mitoEVs and non-mitoEVs showed superoxide production via mitoSOX staining, while the superoxide levels of non-mitoEVs were markedly higher than those of mitoEVs (Fig. 2P). The possible reason is that small EVs are more prone to shed damaged mitochondrial contents, whereas large EVs may contain intact and functional mitochondria (e.g., respiratory-competent mitochondria) (*14*). Moreover, to assess whether these mitochondrial contents are encapsulated within mitoEVs, CFSE-labeled EVs were costained with MDR. As shown in fig. S4 (C and D), a substantial population of $CFSE^+MDR^+$ mitoEVs was detected, suggesting the presence of polarized mitochondria within mitoEVs. In addition, Triton X-100 treatment significantly reduced the events of $CFSE^+MDR^+$ mitoEVs, suggesting that mitoEVs are structurally intact mitochondria-containing vesicles (fig. S4, C and D). Together, these results indicate that healthy muscle tissue–derived mitoEVs are enriched with functional mitochondria and that they may affect the mitochondrial metabolism of recipient cells.

Ti-mitoEVs boost mitochondrial biogenesis in recipient cells

Emerging studies have shown that, under certain conditions, donor cells can transfer their mitochondria to recipient cells through EVs, thereby tuning the metabolic states and biofunctions of target cells (*14*). For example, MSC-derived EVs promote injured tissue repair by transferring mitochondrial contents into recipient cells, such as endothelial cells, lung alveolar epithelial cells, and neuron cells (*20*, *36*, *37*). These findings suggest that mitoEVs may participate in organ-to-organ communication and that they might restore mitochondrial function in energy-deficient injured cells. However, the low efficiency of cell culture–based EV production is still a bottleneck of current EV therapy, and it can be assumed that the yield of mitoEVs in MSCs is much lower. In addition, as a type of stromal cell, MSCs exhibit a greater prevalence of the glycolytic pathway (*38*), which might also restrict their efficiency of mitoEV production. Our results revealed that the yield of Ti-mitoEVs (1-g muscle tissue) was much higher than that of MSC-derived mitoEVs (per 1×10^7 cells) in terms of both particle number (~170-fold) and protein amount (~34-fold) (fig. S9A). In addition, muscle tissue–derived mitoEVs contained higher populations of polarized mitochondria

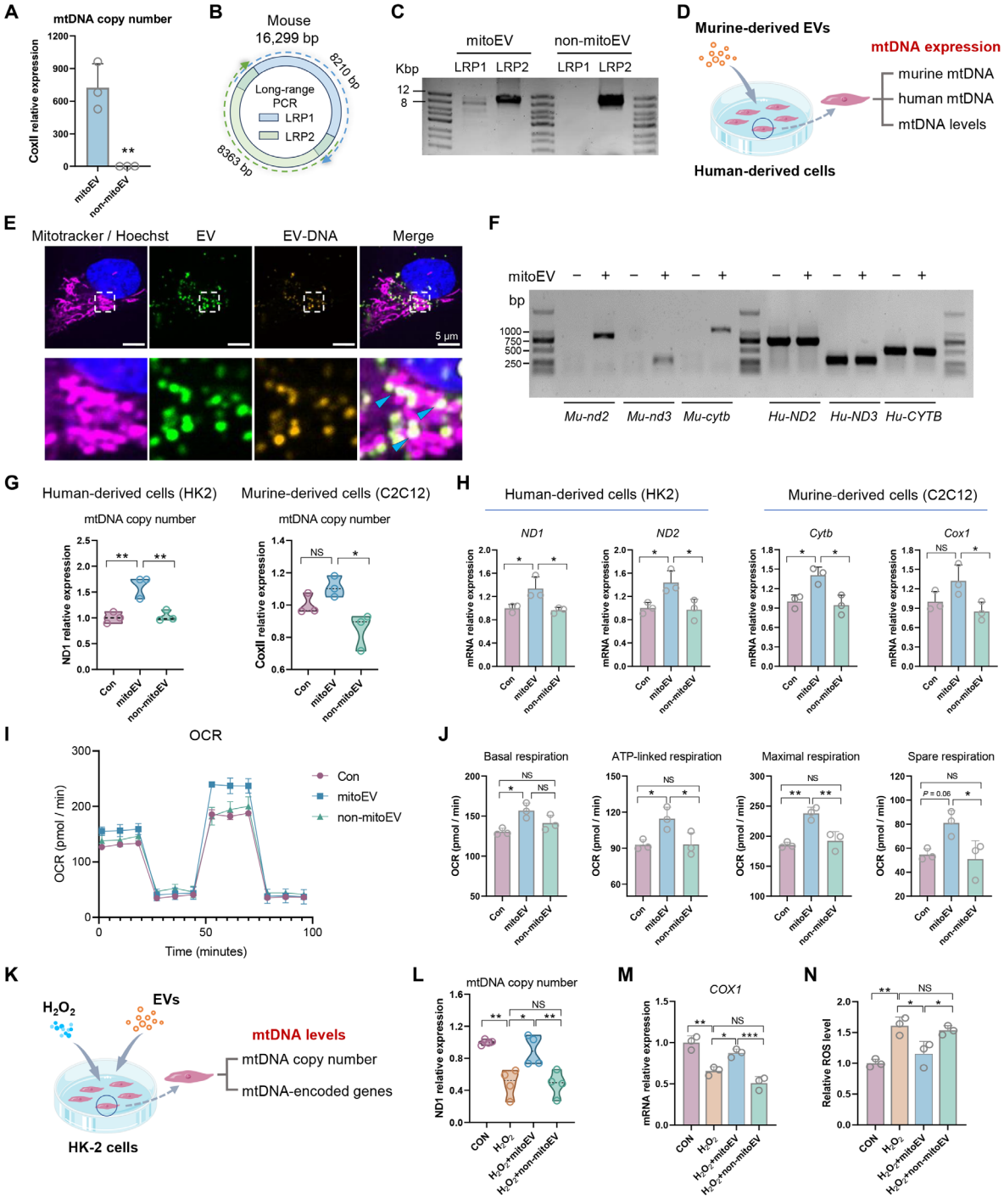

Fig. 3. Evaluating the boosting effect of mitoEV-mediated mitochondrial genome transfer on recipient cells. (**A**) Comparison of mtDNA copy number between mitoEVs and non-mitoEVs ($n = 3$). (**B** and **C**) Schematic diagram (B) and representative agarose gel image (C) of long-range PCR with two amplicons covering the entire mtDNA obtained from mitoEVs and non-mitoEVs. (**D**) Schematic diagram of mitochondrial genome transfer from EVs to recipient cells. (**E**) Confocal images of human cells (HK-2) incubated for 8 hours with murine-derived mitoEVs (scale bar = 5 μm). MitoTracker-labeled mitochondria (magenta), PKH26-labeled EVs (green), EtBr-labeled EV-DNA (yellow), and their colocalization (pale yellow) are shown. (**F**) The expression of murine and human mitochondrial genes in HK-2 cells was determined in the presence or absence of treatment with murine-derived mitoEVs. (**G**) mtDNA copy number levels in recipient cells at 24 hours after mitoEV treatment ($n = 3$). (**H**) qPCR analysis of mtDNA-encoded gene expression in recipient cells at 24 hours after mitoEV treatment ($n = 3$). (**I**) Seahorse analysis (XF24 analyzer) and (**J**) quantitative parameters of mitochondrial respiration in normal HK-2 cells at 24 hours after EV treatment. (**K**) Schematic diagram of mitoEV treatment in the H_2O_2-induced cell mitochondrial injury model. (**L**) mtDNA copy number levels in H_2O_2-induced cells at 48 hours after mitoEV treatment ($n = 3$). (**M**) qPCR analysis of mtDNA-encoded gene expression in H_2O_2-induced cells at 48 hours after mitoEV treatment ($n = 3$). (**N**) Oxidative stress levels in H_2O_2-induced cells at 48 hours after mitoEV treatment ($n = 3$). $^*P < 0.05$, $^{**}P < 0.01$, $^{***}P < 0.001$, and NS = not significant.

but exhibited similar mitochondrial superoxide levels than MSC-derived mitoEVs did (fig. S9, B and C). These results indicate that Ti-mitoEVs may be more ideal for therapeutic applications.

The biogenesis of mitochondrial contents is tightly controlled by a complex signaling network in response to the cellular metabolic demand, and the mitochondrial genome contributes to the generation of OXPHOS complexes (*39*). We next determined whether Ti-mitoEVs could transfer mitochondrial contents (e.g., mtDNA) to recipient cells. To this end, human-derived cell lines (HK-2 cells) were incubated with murine-derived mitoEVs for 8 hours (Fig. 3D). We observed the colocalization of mitoEVs (green), mitoEV-carried mtDNA (yellow), and the mitochondria of HK-2 cells (magenta), implying that mitoEVs might fuse with the mitochondria of recipient cells and thus transfer mtDNA into them (Fig. 3E). Previous studies have revealed the fusion of mitochondria-carrying EVs with the native mitochondria of target cells, suggesting that it is a potential route of intracellular metabolic regulation (*32*). Human cells (HK-2 cells) incubated with murine tissue–derived mitoEVs simultaneously exhibited intramitochondrial murine mtDNA (e.g., *Mu-nd2*, *Mu-nd3*, and *Mu-cytb*) and human mtDNA (e.g., *Hu-ND2*, *Hu-ND3*, and *Hu-CYTB*), confirming the ability of mitoEVs to transfer the mitochondrial genome into the mitochondria of recipient cells at 8 hours (Fig. 3F). In addition, mitoEV treatment up-regulated the levels of mtDNA copy numbers in recipient cells (Fig. 3G) and mtDNA-encoded genes (e.g., *ND1*, *ND2*, *Cytb*, and *CoxI*) expression in human-derived cells (HK-2 cells) or murine-derived cells (C2C12 cells) compared to non-mitoEVs at 24 hours (Fig. 3H), suggesting that they might primarily enhance mitochondrial transcription and its associated mitochondrial biogenesis in recipient cells. It has been reported that mtDNA can be integrated into mitochondrial biogenesis pathways and regulate mitochondrial metabolism in concert with nuclear-encoded mitochondrial factors (*39*). Consequently, mitoEVs treatment significantly increased the mitochondrial respiratory capacities (including basal, ATP-linked, maximal, and spare respiration) of normal HK-2 cells at 24 hours, whereas this effect was minimal in the non-mitoEVs group (Fig. 3, I and J), suggesting that mitoEVs treatments can boost mitochondrial biogenesis to enhance OXPHOS in HK-2 cells. In addition, in an oxidative stress (H_2O_2)–induced cell mitochondrial injury model, mitoEV treatment was more effective at restoring mtDNA copy numbers and mitochondrial gene expression (e.g., *COXI*) in damaged cells than non-mitoEV treatment was at 48 hours (Fig. 3, K to M), confirming that mitoEVs can restore mitochondrial biogenesis and function in injured recipient cells. As a result, mitoEV treatment alleviated the oxidative stress induced by hydrogen peroxide (Fig. 3N). These results indicate that mitoEVs can boost mitochondrial biogenesis in recipient cells via mitochondrial genome transfer.

SEC-purified Ti-mitoEVs retain mitochondrial components and bioactivities

Considering that UC alone may co-isolate non-EV contaminants and potentially influence the biological outcomes of EV preparations, size exclusion chromatography (SEC) was used to further purify the EV preparations obtained from UC, as SEC has been recognized as one of the most reliable methods for purifying EVs without introducing additional contaminants (*40*). As shown in Fig. 4 (A to C), the mitoEVs or non-mitoEVs preparations presented normal-like distributions of particle and protein concentrations, while the majority of the particles and proteins were eluted within fractions 3 to 6, with peak concentrations observed in fraction 4. The cumulative 50% data point for both particle and protein concentrations was also located around fraction 4, which coincided with the center of the particle and protein peaks (Fig. 4, B and C, and fig. S12, A and B), suggesting that fractions 3 to 6 might represent the EV-enriched fraction. Thus, eluent fractions 3 to 6 were collected as the SEC-purified EV (EV^{SEC}) fraction, while fraction 7 and beyond were considered the co-isolated contaminant fraction. The purified $mitoEV^{SEC}$ or non-$mitoEV^{SEC}$ expressed positive markers (e.g., TSG101 and CD63) without negative marker (e.g., GM130) expression (Fig. 4D). Similar to the mitoEV preparations, the purified $mitoEV^{SEC}$ presented higher mtDNA copy numbers and mitochondrial protein levels (e.g., MIM, MOM, and matrix proteins) compared to non-$mitoEV^{SEC}$ (Fig. 4, E and F, and fig. S10). In addition, Triton X-100 treatment significantly reduced both $CFSE^+$ $mitoEV^{SEC}$ events and $CFSE^+MDR^+$ $mitoEV^{SEC}$ events (fig. S11, A to D). These results demonstrate that our mitoEV preparations indeed contain abundant mitochondrial contents (e.g., mtDNA and mito-proteins).

Next, the effect of purified EV^{SEC} on the mitochondrial metabolism of recipient cells was assessed. To evaluate the role of $mitoEV^{SEC}$ in functional mitochondrial genome transfer, murine-derived $mitoEV^{SEC}$ was added to human-derived cells (HK-2 cells), and then, murine mtDNA copy numbers in HK-2 cells were measured (Fig. 4, G to I). Like those in the mitoEV group, HK-2 cells in the $mitoEV^{SEC}$ group showed significantly greater murine mtDNA copy numbers than those in the control group, contaminant group, or non-$mitoEV^{SEC}$ group at 24 hours after treatment (Fig. 4H). The colocalization of $mitoEV^{SEC}$ (green), $mitoEV^{SEC}$-carried mtDNA (orange), and the mitochondria (magenta) of HK-2 cells was observed (Fig. 4I), which indicates that $mitoEV^{SEC}$ can transfer mitochondrial contents (e.g., mtDNA) into recipient cells, which is consistent with previous reports (*32*). The impact of $mitoEV^{SEC}$ treatment on the mitochondrial metabolism of recipient cells was also assessed via Seahorse analysis. In line with the results of mitoEVs, $mitoEV^{SEC}$ treatment also increased mitochondrial respiration (e.g., maximal respiration) in normal HK-2 cells at 24 hours, whereas this effect was minimal in the non-$mitoEV^{SEC}$ group (Fig. 4, J and K). In addition, $mitoEV^{SEC}$ treatment was more effective at restoring mitochondrial respiratory capacity (e.g., basal and maximal respiration) in injured HK-2 cells than non-$mitoEV^{SEC}$ treatment at 24 hours (Fig. 4, L to N). Together, these results verify that $mitoEV^{SEC}$ treatment can boost mitochondrial metabolism in recipient cells and that this effect is at least partially due to mtDNA transfer.

Furthermore, whether co-isolated contaminants affect the mitochondrial metabolism of recipient cells was assessed. Compared with the $mitoEV^{SEC}$ fractions, the contaminant fractions from SEC separation showed negligible levels of mitochondrial proteins and positive EV markers (e.g., HSP70 and TSG101) expressions (fig. S12, C and D), indicating that the mitochondrial components of our mitoEV preparations are unlikely to be due to co-isolated contaminants. Moreover, compared with the $mitoEV^{SEC}$ treatment, the co-isolated contaminants alone failed to enhance mitochondrial respiration in recipient HK-2 cells at 24 hours after treatment (fig. S12, E and F). These results again indicate that our mitoEV preparations contain abundant mitochondrial contents and effectively enhance the mitochondrial metabolism of recipient cells, with this effect mainly attributed to the mitoEVs themselves rather than co-isolated contaminants. On the basis of these results, considering the low EV yield of SEC separation and the high EV dosage required for therapeutic purposes, we

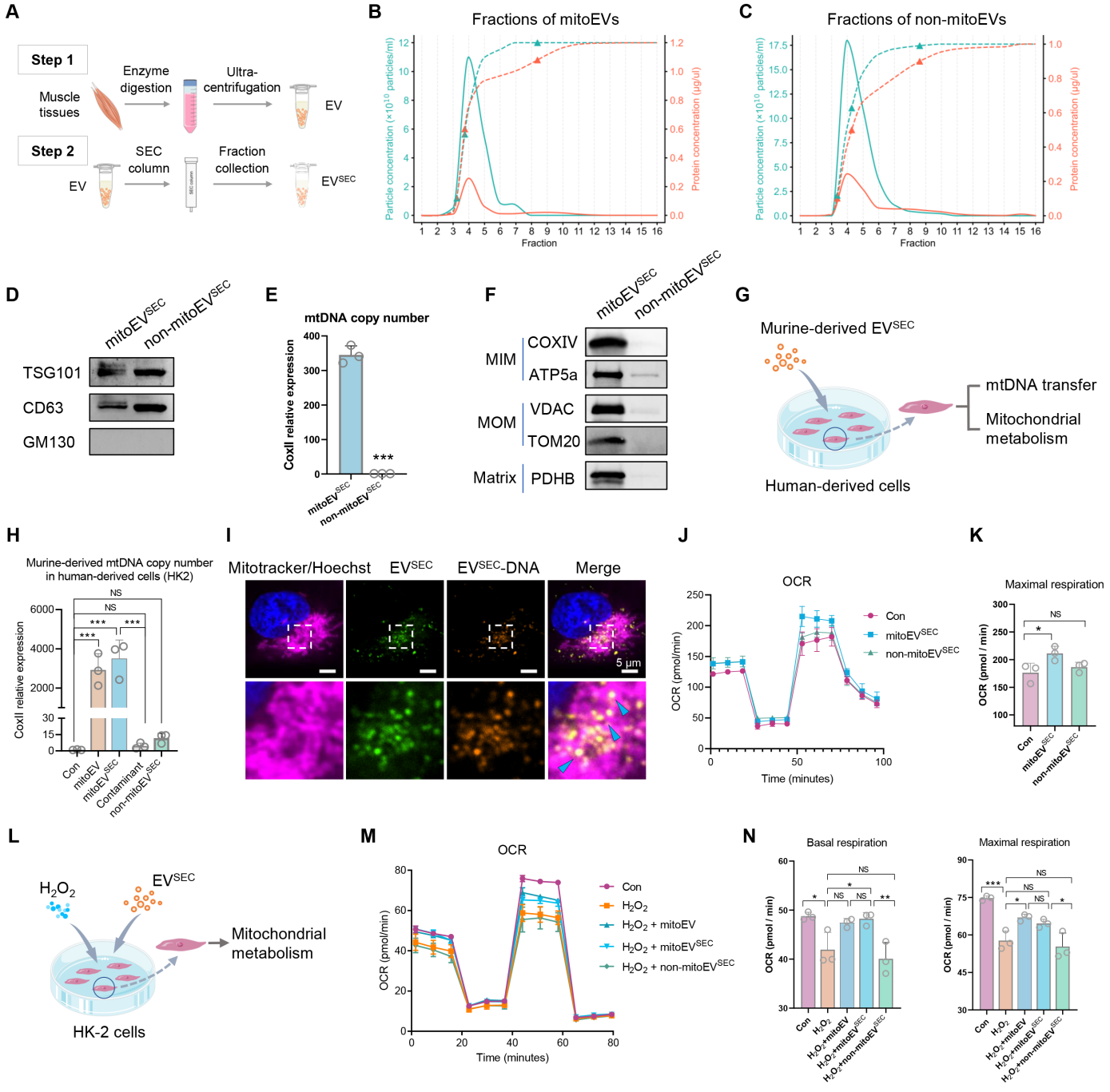

Fig. 4. Evaluating the boosting effect of purified mitoEV (mitoEV^{SEC})–mediated mitochondrial genome transfer on recipient cells. (**A**) Schematic diagram of EV purification using a SEC column. (**B** and **C**) Fraction distributions of particle (green) and protein (orange) concentrations in different EV samples. (**D** to **F**) Comparison of EV markers (D), mtDNA copy number (E), and mitochondrial protein content (F) between mitoEV^{SEC} and non-mitoEV^{SEC}. (**G**) Schematic diagram of mitochondrial genome transfer from EVs to recipient cells. (**H**) Murine mtDNA copy number levels in recipient human cells after 24 hours of EV treatment ($n = 3$). (**I**) Confocal images of human cells (HK-2) incubated for 8 hours with murine-derived mitoEV^{SEC} (scale bar = 5 μm). (**J** and **K**) Seahorse analysis (XF24 analyzer) (J) and quantitative parameters (K) of mitochondrial respiration in normal HK-2 cells at 24 hours after purified EV treatment ($n = 3$). (**L**) Schematic diagram of EV treatment in the H_2O_2-induced cell mitochondrial injury model. (**M** and **N**) Seahorse analysis (XF96 analyzer) (M) and quantitative parameters (N) of mitochondrial respiration in H_2O_2-induced injured HK-2 cells at 24 hours after EV treatment ($n = 3$). *$P < 0.05$, **$P < 0.01$, ***$P < 0.001$, and NS = not significant.

decided to use mitoEVs for therapeutic purposes in subsequent in vivo tests.

Ti-mitoEVs alleviate mitochondrial damage and promote tissue repair

The in vivo therapeutic effects of mitoEVs were further assessed via both acute and chronic forms of tissue injury characterized by mitochondrial injury (Figs. 5A and 6A). Skeletal muscle function relies heavily on mitochondria for energy generation, while acute skeletal muscle injury (AMI) caused by toxins (e.g., cardiotoxin) can disrupt mitochondrial function and aggravate muscle damage (*24*, *41*). The mouse AMI model induced by intramuscular (i.m.) cardiotoxin injection clearly exhibited myofiber degeneration and mitochondrial network destruction on day 3 postinjection (Fig. 5, A to G, and fig. S13, A and B). In contrast, mitoEV treatments (i.m. injection) effectively attenuated muscle injury in AMI mice, as evidenced by reduced myofiber lysis and preserved basal lamina (e.g., laminin) integrity compared with those in the AMI alone group (Fig. 5, B to E, and fig. S13, A and B). The muscles of AMI mice that received mitoEV therapy exhibited higher levels of mitochondrial biogenesis [indicated by transcription factor A, mitochondrial (TFAM)] and mitochondrial mass (indicated by TOM20) compared to the AMI alone group (Fig. 5, F and G), confirming that mitoEV therapy can effectively alleviate mitochondrial damage in skeletal muscle after AMI. The i.m. injected 1,1′-Dioctadecyl-3,3,3′,3′-tetramethylindodicarbocyanine perchlorate (DiD)-labeled mitoEVs (red) colocalized with myofibers (green) or immune cells ($Ly6C^+$ monocytes, green) in the injured muscle tissue (fig. S14), suggesting that mitoEVs might arrive both resident muscle cells and infiltrated immune cells to exert therapeutic effects.

Mitochondria are also vital regulators of inflammation, as damaged mitochondria can serve as damage-associated molecular patterns to induce cytokine release and proinflammatory cell recruitment and activation, which in turn aggravate tissue injury (*41*). Consistently, we found that mitoEV treatment also reduced the levels of cytokine (e.g., *Icam*, γ-*Ifn*, *Il-6*, and *Tnf*-α) and proinflammatory cell (e.g., $F4/80^+$ macrophages) infiltration in the injured muscle of AMI mice (Fig. 5, H and I, and fig. S13C). Although less effective than mitoEVs, non-mitoEVs showed certain potential to reduce inflammation and myofiber damage in injured muscles of AMI mice (Fig. 5, B to E, H, and I; and fig. S13, A to C). However, non-mitoEV treatments had significantly lower efficacy in mitigating mitochondrial damage in the injured muscles of AMI mice compared to mitoEVs (Fig. 5, F and G). The partial beneficial role of non-mitoEVs in reducing muscle injury might be because they also contain some protein components related to the processes of muscle structure development and myofiber assembly processes (fig. S5, D to F). These results indicate that mitoEVs have superior efficacy in alleviating mitochondrial damage and promoting muscle repair.

The kidneys are also among the major high-energy-demand organs in the body (*42*), while mitochondrial damage, such as mitochondrial stress and impaired ATP production, is increasingly recognized as a key player in chronic kidney disease (CKD) (*43*). CKD is a long-term condition characterized by a gradual loss of kidney function that can affect more than 800 million people worldwide, but there is no effective therapy currently available in the clinic (*44*). Thus, the therapeutic effects of mitoEV treatments on CKD were also assayed in vivo (Fig. 6A). The in vivo distribution of systemically [intraperitoneally (i.p.)] injected Cy7-labeled mitoEVs was assayed. Positive signals of mitoEVs could be observed in major organs (including kidneys) of mice, but there was no significant difference in the renal signals between mitoEVs and non-mitoEVs (fig. S15). In addition, the i.p. injected DiD-labeled mitoEVs (green) were found to colocalize with renal parenchymal cells (AQP^+ tubular epithelial cells, red) and innate immune cells ($Ly6C^+$ monocytes, red) in the kidney tissues of CKD mice (fig. S16). These findings indicate that the administered mitoEVs might arrive both injured tissue cells and infiltrated immune cells in vivo. It has been reported that innate immune cells might phagocytose injected lipid nanoparticles and then transfer them to injured tissue cells (*45*), which may explain our findings to some extent. However, the exact cell types and the dynamic process of mitoEV uptake in vivo are complicated and need further investigation.

In folic acid–induced CKD mice, mitoEV therapy significantly reduced the degree of renal fibrosis, as indicated by lower levels of extracellular matrix (ECM) (*Col1a1* and *Fn*) expression and smaller positive areas of Masson and picrosirius red staining compared to the CKD alone group, and it showed superior antifibrotic potency than non-mitoEVs did (Fig. 6, B and C, and fig. S17, A to C). Moreover, mitoEV treatments effectively restored renal mitochondrial biogenesis (TFAM expression) and mitochondrial mass (*Atp5a* and TOM20) levels in CKD mice, whereas non-mitoEV treatments had lower renoprotective effects (Fig. 6, D to F). Subsequently, mitoEV treatments reduced renal cytokine (e.g., *Icam*, *Tnf*-α, *Il-1*β, and *Il-6*) expression and proinflammatory cell (e.g., $CD68^+$ macrophages) infiltration in CKD mice, and mitoEVs also exhibited higher anti-inflammatory potency than non-mitoEVs did (Fig. 6, G to I, and fig. S17D). The differences in therapeutic efficacy between mitoEVs and non-mitoEVs may be due to their different compositions, particularly their functional mitochondrial contents. Together, our results indicate that mitoEV treatment can alleviate mitochondrial injury in diverse forms of tissue injury in vivo.

Ti-mitoEVs exert tissue-protective effects through boosting mitochondrial metabolism

Having found the tissue protective potency of Ti-mitoEVs therapy in vivo, we further explored its underlying mechanism via RNA sequencing (RNA-seq). PCA plot and heatmap revealed altered gene expression profiles in the injured kidneys of CKD mice compared with those of control mice, which could be partially reversed after mitoEV or non-mitoEV treatment (fig. S18). Compared with those of control mice, the kidney tissues of CKD mice presented elevated gene expression related to kidney injury (e.g., *Havcr1* and *Lcn2*), mitochondrial dysfunction (e.g., *Cyp24a1*, *Ppargc1a*, and *mt-Nd5*), chronic inflammation (e.g., *Nfkbia* and *Cd68*), and renal fibrosis (e.g., *Fn1*, *Col3a1*, and *Col1a1*) (fig. S19, A to F). Compared with those in the CKD alone group, the differentially expressed genes (DEGs) induced by mitoEV (885 up-regulated and 2346 down-regulated) and non-mitoEV (188 up-regulated and 496 down-regulated) treatments were identified (Fig. 7A). The up-regulated DEGs of the mitoEV group were enriched mainly in mitochondria-related components (e.g., MIM and mitochondrial matrix) and energy metabolism–related pathways (e.g., ion transport, ATP synthesis, ETC, and mitochondrial transmembrane) (Fig. 7, A to E), whereas the down-regulated DEGs of the mitoEV group were enriched mainly in immune response (e.g., inflammation, immune cell activation, and cytokine production) and fibrotic processes (e.g., ECM proteins) (Fig. 7, A, F, and G). Non-mitoEV treatment also reduced the expression of some genes

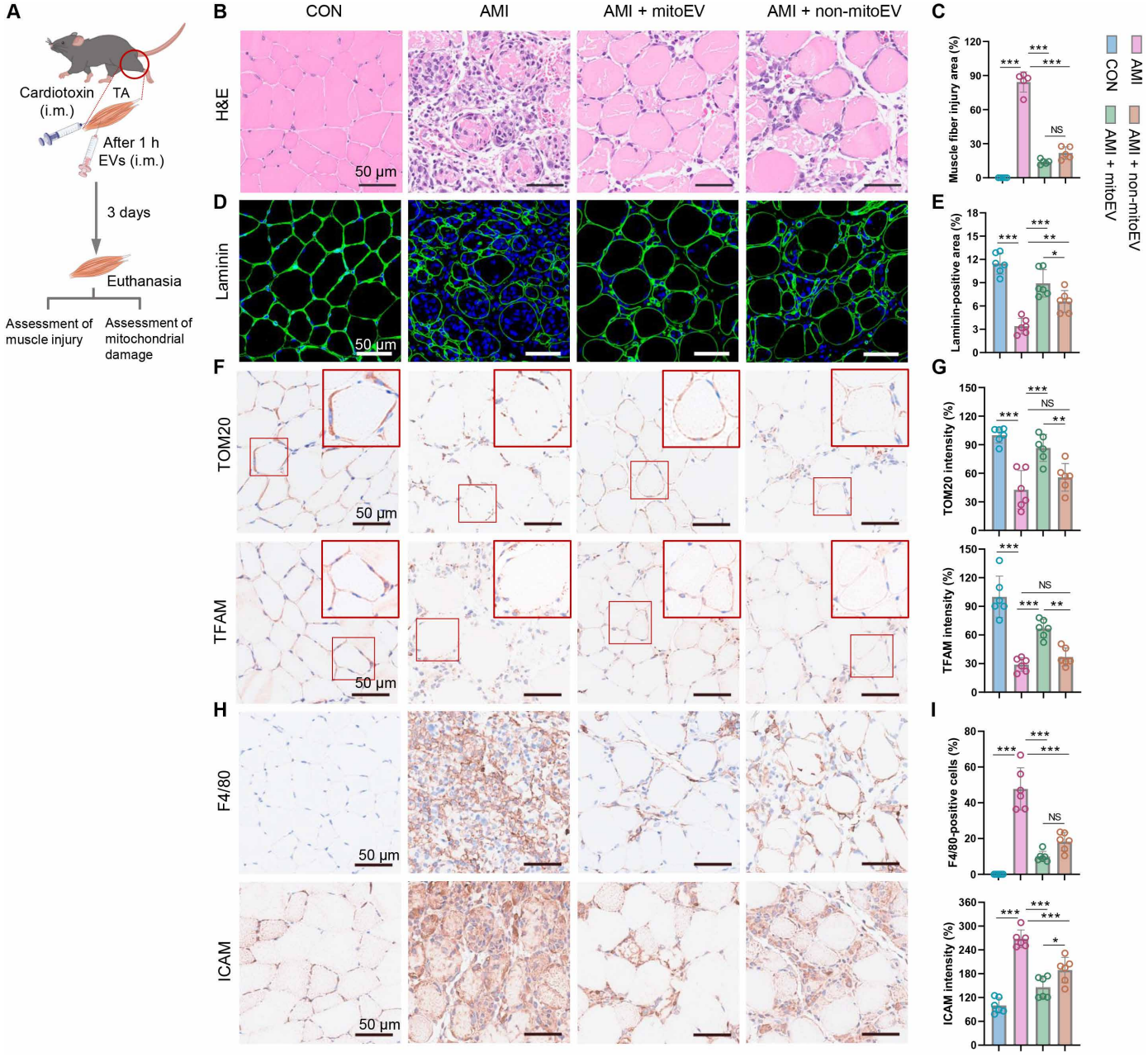

Fig. 5. Evaluating the repair efficacy of mitoEVs in AMI. (**A**) Experimental scheme of the AMI study. (**B**) Representative H&E staining images of muscle on day 3 after AMI (scale bar = 50 μm). (**C**) Quantitative analysis of the muscle injury area ($n = 5$). (**D**) Representative LN IF staining images of muscle on day 3 after mitoEV treatment (scale bar = 50 μm). (**E**) Quantitative analysis of LN expression in muscle ($n = 6$). (**F**) IHC staining images of TFAM and TOM20 on day 3 after AMI (scale bar = 50 μm). (**G**) Quantitative analysis of TFAM and TOM20 protein expression ($n = 6$). (**H**) IHC staining images of F4/80 and ICAM on day 3 after AMI (scale bar = 50 μm). (**I**) Quantitative analysis of F4/80 and ICAM protein expression ($n = 6$). $^{*}P < 0.05$, $^{**}P < 0.01$, $^{***}P < 0.001$, and NS, not significant.

associated with certain pathways, such as inflammatory response and fibrosis processes, but non-mitoEV treatment showed much lower efficacy in restoring decreased mitochondrial metabolism–related gene expression in the kidneys of CKD mice (Fig. 7A and fig. S20). These results suggest that Ti-mitoEVs may promote tissue injury repair by restoring mitochondrial metabolism.

Boosting mitochondrial metabolism via exercise enhances Ti-mitoEV secretion

To explore the potent role of mitoEVs secretion in regulating the mitochondrial metabolism of skeletal muscle in vivo, we evaluated the changes in mitoEVs via a mouse high-intensity interval training (HIIT) model (Fig. 8A). Notably, exercise, such as HIIT, is a powerful

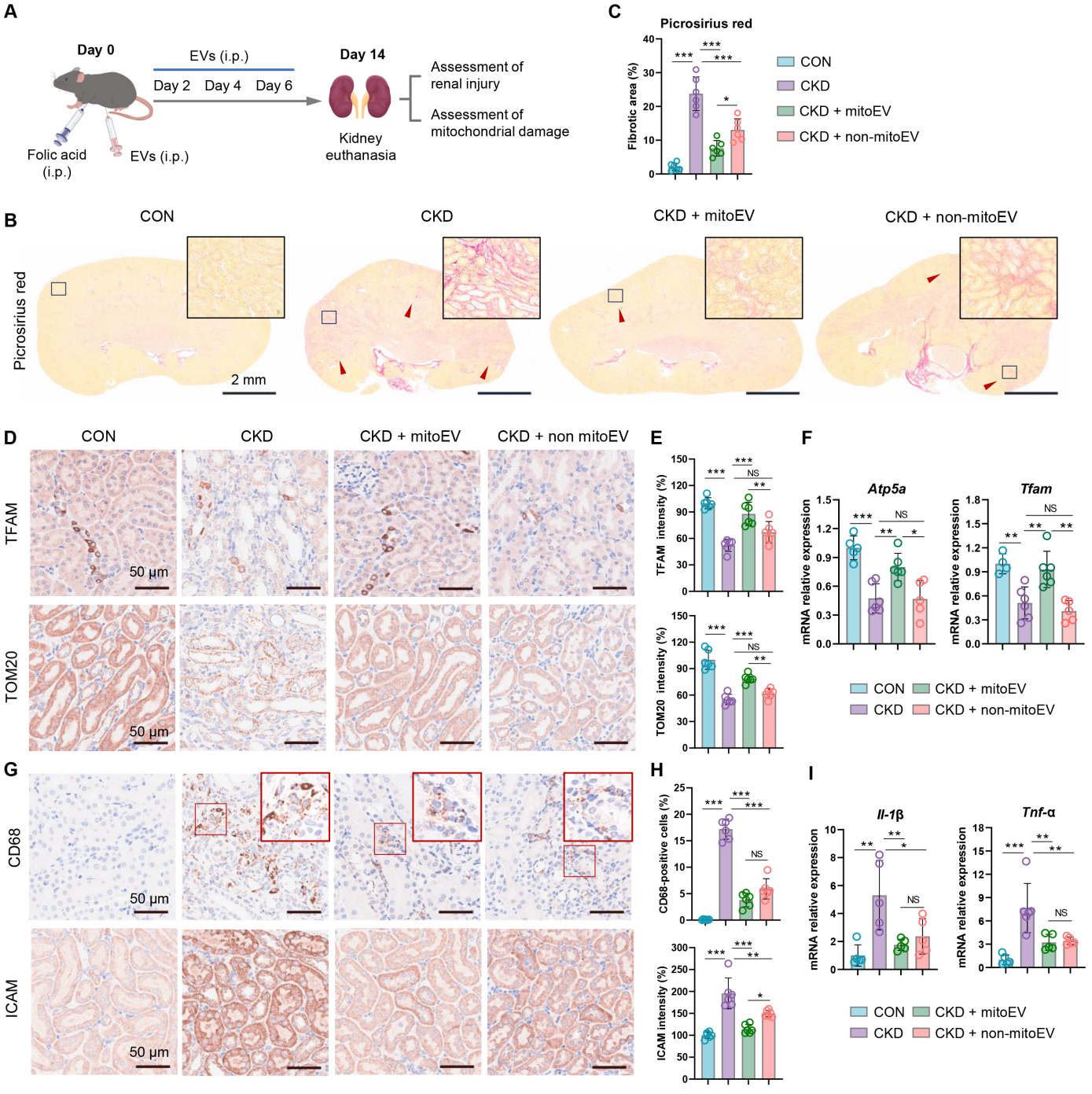

Fig. 6. Evaluating the repair efficacy of mitoEVs in CKD. (**A**) Experimental scheme of the CKD study. (**B**) Representative picrosirius red stained images of kidneys on day 14 after CKD (scale bar = 2 mm). (**C**) Quantitative analysis of the renal fibrosis area ($n = 6$). (**D**) IHC staining images for TFAM and TOM20 on day 14 after CKD (scale bar = 50 μm). (**E**) Quantitative analysis of TFAM and TOM20 protein expression ($n = 6$). (**F**) qPCR analysis of mitochondrial-related gene expression in the kidneys of the mice ($n = 6$). (**G**) Images of IHC staining for CD68 and ICAM on day 14 after CKD induction (scale bar = 50 μm). (**H**) Quantitative analysis of CD68 and ICAM protein expression ($n = 6$). (**I**) qPCR analysis of inflammation-related gene expression in the kidneys of the mice ($n = 6$). $^*P < 0.05$, $^{**}P < 0.01$, $^{***}P < 0.001$, and NS = not significant.

stimulus for increasing mitochondrial metabolism (e.g., mitochondrial biogenesis and energy metabolism) in skeletal muscle (*46*), and increased EV secretion was also found in skeletal muscle during exercise (e.g., cycling) (*12*, *47*). Our results revealed that HIIT markedly altered the gene expression profile of mouse skeletal muscle, and the 263 up-regulated genes [fold change (FC) > 1.5, $P < 0.05$] were enriched mainly in pathways related to metabolic regulation (e.g., mitochondrial energy metabolism, regulation of ion transport, and regulation of secretion by cells), regulation of cell communication, and immune system development (Fig. 8, B to D). In line with previous reports (*46*, *48*), multiple critical regulators of mitochondrial biogenesis (e.g., *Pgc-1α*, *Ppara*, and *Sirt1*) were up-regulated

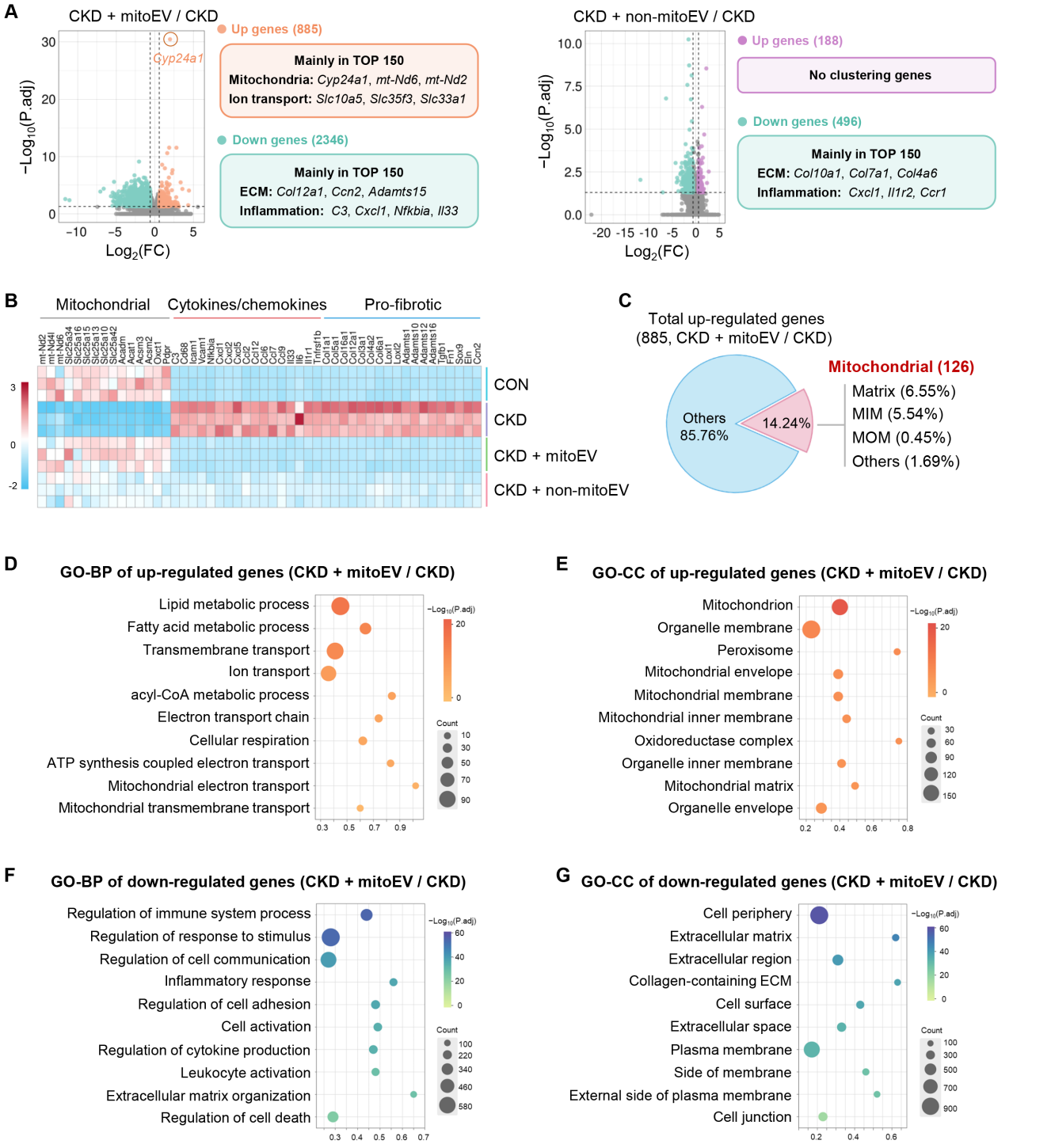

Fig. 7. Modes of action of mitoEVs in promoting renal repair after CKD. (**A**) Volcano plot showing the DEGs in CKD kidneys treated with mitoEVs and non-mitoEVs. (**B**) Heatmap of mitochondrial-, cytokine/chemokine-, and fibrosis-related gene expression in CKD renal treated with mitoEVs. (**C**) Proportion of mitochondrial proteins among the DEGs in CKD kidneys treated with mitoEVs. (**D** and **E**) GO biological process (D) and cellular component (E) analyses of the up-regulated DEGs in CKD kidneys treated with mitoEVs. (**F** and **G**) GO biological process (F) and cellular component (G) analyses of the down-regulated DEGs in CKD kidneys treated with mitoEVs. FC > 1.5 and *P*-adjusted <0.05.

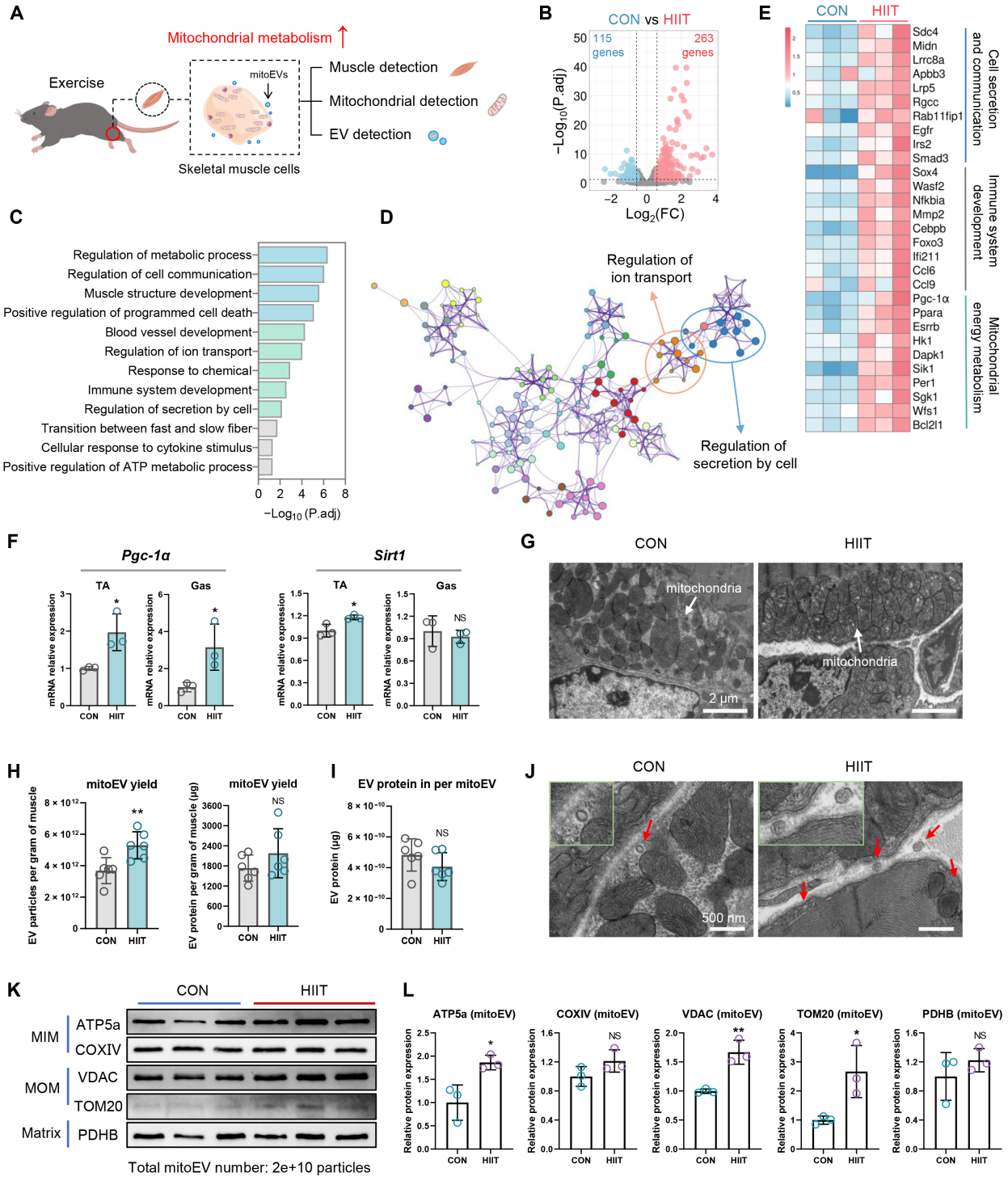

Fig. 8. mitoEV secretion is a natural regulator of tissue mitochondrial metabolism. (**A**) Schematic diagram of changes in mitochondrial metabolism in mice after exercise. (**B**) Volcano plots showing the number of DEGs in muscle after HIIT (FC > 1.5 and *P*-adjusted <0.05). (**C** to **E**) GO analysis (C), interaction network (D), and heatmap (E) of the DEGs between the CON group and HIIT group. (**F**) qPCR analysis of mitochondrial biogenesis-related gene expression in the muscle of mice ($n = 3$). (**G**) Representative TEM images of mitochondrial morphology (scale bar = 2 μm). (**H**) Muscle mitoEV yield after HIIT ($n = 6$). (**I**) EV protein amounts at the single mitoEV level ($n = 6$). (**J**) Representative TEM image of endogenous EVs within mouse skeletal muscle tissues after HIIT (the red arrow indicates EVs; scale bar = 500 nm). (**K**) Mitochondrial protein content of mitoEVs after HIIT ($n = 3$). (**L**) Quantitative analysis of mitochondrial protein expression ($n = 3$). $^*P < 0.05$, $^{**}P < 0.01$, $^{***}P < 0.001$, and NS = not significant.

after HIIT (Fig. 8, E and F). TEM images revealed that the mitochondria in the muscle tissues of the HIIT group were more aggregated and densely arranged than those in the control group were (Fig. 8G), indicating that acute exercise can stimulate mitochondrial metabolism, such as mitochondrial dynamics, in skeletal muscle. The enhanced mitochondrial fusion of muscle tissues during acute exercise is likely due to the high energy demand in a short period (*49*).

Furthermore, multiple pathways related to cell secretion and cell communication were also up-regulated in the muscle of the HIIT group compared with the control group (Fig. 8, C to E), suggesting that the mitoEV secretion process might also be enhanced in response to mitochondrial stimulation (e.g., exercise). TEM images revealed more EVs present in the interstitial spaces between the tissue cells within mouse skeletal muscle post-HIIT, and the muscle tissues of the HIIT group presented increased mitoEV yields as well as increased levels of many mitochondrial proteins (e.g., ATP5a, COXIV, VDAC, TOM20, and PDHB) in mitoEVs compared with those of the control group (Fig. 8, H to L, and fig. S21). These results collectively indicate that Ti-mitoEVs release may function as an intrinsic mechanism of mitochondrial regulation in muscle, which may provide a tool for tuning mitochondrial metabolism in target cells. In addition, the beneficial effect of exercise on increasing the yield or biological activities of Ti-mitoEVs might further improve the potential of Ti-mitoEV–based therapies for regenerative medicine and promote their future clinical translation. However, the detailed effects of training parameters (e.g., type, intensity, and duration) on muscle mitoEV secretion (e.g., amounts and compositions) remain elusive and need to be explored in future studies.

In the present study, inspired by the natural process of EV-mediated intercellular mitochondria transfer and its vital role in the regulation of cellular metabolism and tissue homeostasis, we directly isolated mitoEVs from healthy muscle tissues and explored their potential effects on tissue injury repair (Fig. 9). We found that tissue-derived mitoEV subpopulations contain almost all types of mitochondrial proteins and the whole mitochondrial genome and that they can boost mitochondrial biogenesis in recipient cells by transferring functional mitochondrial components (e.g., the mitochondrial genome). On the basis of previous reports and our findings, Ti-mitoEVs likely act as a type of natural nanoregulator of mitochondrial metabolism in vivo. Owing to this unique property, mitoEVs may serve as potent mitochondrial replenishment therapies for regenerative medicine by restoring mitochondrial biogenesis and energetic metabolism while alleviating oxidative stress in injured tissue cells. In addition, Ti-mitoEV therapy may have some advantages over current therapies, such as mitochondrial transplantation and small chemicals. For example, mitochondrial transplantation therapy faces several challenges, such as difficulty storing, shipping and a potent immune response, and isolated mitochondria are prone to rapid inactivation in the harsh microenvironment (oxidative stress and inflammation) of injured tissues (*50*). In contrast, the unique phospholipid bilayer structure of Ti-mitoEVs can protect encapsulated functional mitochondria from external damage, thereby offering greater stability and feasibility for storage and clinical use. As tissue cell–derived natural nanovesicles and an endogenous means of regulating mitochondrial metabolism, Ti-mitoEVs may offer higher biosafety, bioavailability, and tissue/cell specificity than small

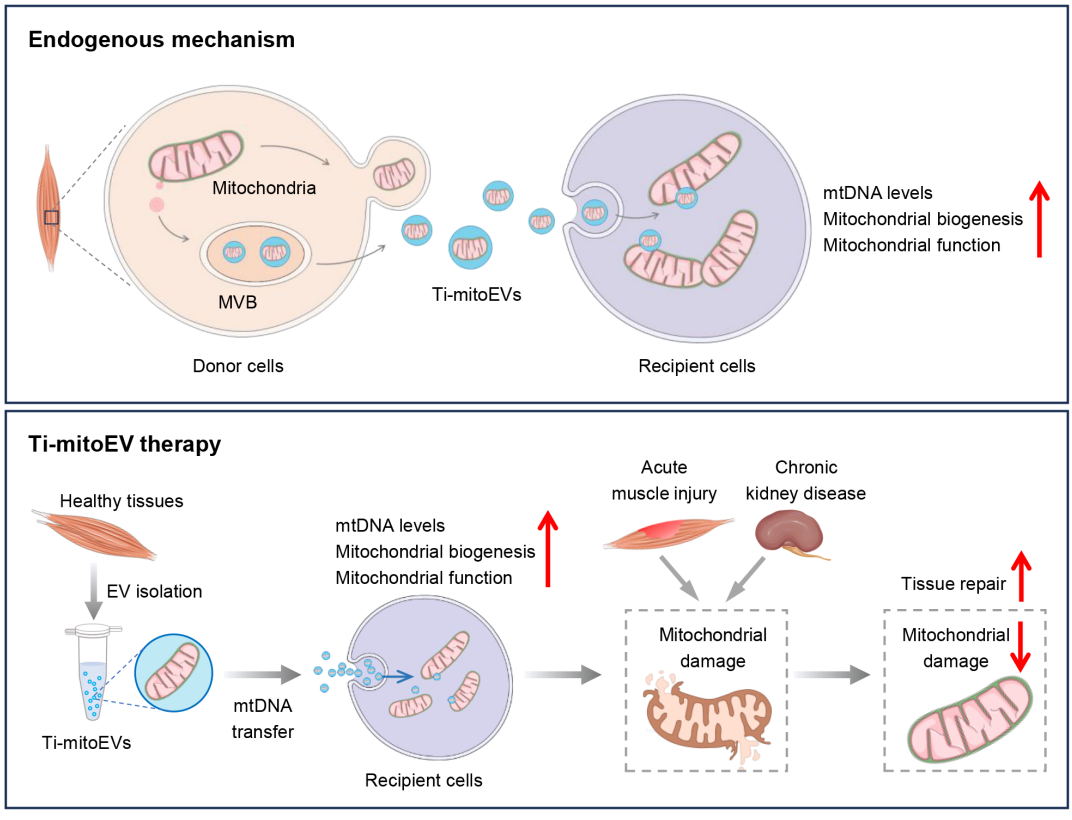

Fig. 9. Schematic diagram of Ti-mitoEV therapy. Inspired by natural EV-mediated mitochondrial transfer and its role in cellular metabolism and tissue homeostasis, Ti-mitoEVs act as nanoboosters for mitochondrial biogenesis, offering potential for regenerative medicine in tissue injuries linked to mitochondrial dysfunction.

chemicals do. Furthermore, the tissue repair potency of mitoEVs can be further improved by engineering methods, such as modification with targeted molecules or therapeutic payloads and integration with bioactive materials. Therefore, mitoEVs may serve as a mitochondrial replenishment therapy for regenerative medicine and hold potential for future clinical translation.

Although the results showing that Ti-mitoEVs promote mitochondrial function and tissue repair are encouraging, several questions remain elusive and need to be addressed in future studies. For example, the exact cell origin of Ti-mitoEVs is still unclear, as various cell types within muscle tissue can secrete EVs. We have shown that mitoEVs exert tissue repair effects by boosting mitochondrial biogenesis, but non-mitoEV also play a tissue protective role to some extent, which is likely due to the different compositions of mitoEVs and non-mitoEVs, and their different functions or mechanisms of action in tissue repair need further exploration. Moving forward, identifying the specific effector cargos of Ti-mitoEV therapy and then loading these effectors into EV "mimetic" monocultures may facilitate future clinical translation (*51*). In addition, as a proof-of-concept study, the therapeutic effects of Ti-mitoEVs have been assessed in only two types of experimental animal models, and their role in tissue repair needs to be verified in additional types of tissue injury and large animal models. Although the unique lipid bilayer structure of EVs can preserve their bioactive cargos, the optimal storage conditions for maintaining the structural integrity and biological activity of mitoEVs are still unclear. Recent studies have shown that EVs can be preserved under specific conditions, such as freezing at −80°C in buffer solutions or lyophilization without significant loss of functionality (*52*, *53*), and such methods might also be adapted for long-term storage of mitoEVs for clinical trials. Therefore, establishing an optimized storage protocol for mitoEVs and evaluating the impact of different storage conditions on their therapeutic efficacy require further research.

To ensure the safety and efficacy of mitoEV-based therapies, several parameters, such as the purity of mitoEV preparations, the integrity and functionality of mitochondrial contents, and the absence of microbial contamination or endotoxins, should be rigorously assessed. For instance, the absence of contaminants (e.g., cellular debris and non-EV particles) should be confirmed via electron microscopy or flow cytometry analyses (*54*). The presence of EV-specific markers (e.g., TSG101 and CD63) and the absence of negative markers (e.g., GM130 and calnexin) should also be verified (*52*). The integrity and functionality of the mitochondrial composition of mitoEVs should be assessed via the use of mitochondria-specific dyes, MMP indicators, and functional cell assays (*16*, *55*). In addition, sterility and endotoxin tests are essential to ensure compliance with regulatory standards for clinical applications (*52*, *53*). Together, addressing these quality assurance criteria will be critical for the successful translation of Ti-mitoEVs into clinical practice. Nevertheless, the findings of this study indicate that Ti-mitoEVs can serve as natural nanoboosters of mitochondrial biogenesis and may provide insights into advanced regenerative medicine for diverse forms of tissue injuries associated with mitochondrial injury.

MATERIALS AND METHODS

Animals

All animal experiments were performed following the Guidelines of the National Institutes of Health on the Use of Laboratory Animals and were approved by the Animal Care and Use Committee of West China Hospital, Sichuan University (permit no. 20220210002). Healthy C57BL/6 mice (male, 6 to 8 weeks) and Sprague-Dawley (SD) rats (male, 1 to 2 weeks) were purchased from Byrness Weil Biotech Ltd. (Chengdu, China) and housed in a special pathogen–free facility.

Cell culture

Bone marrow–derived MSCs were collected from neonatal (1 to 2 weeks) SD rats and cultured in Dulbecco's Modified Eagle Medium (DMEM; Gibco, CA, USA) supplemented with 10% (v/v) fetal bovine serum (FBS; Gibco) and 1% penicillin-streptomycin (Beyotime Biotechnology, Shanghai, China). Human renal proximal tubule epithelial cell lines (HK-2) were cultured in DMEM/F-12 (Gibco) supplemented with 10% FBS and 1% penicillin-streptomycin. Mouse myoblast cell lines (C2C12) were cultured in DMEM (Gibco) supplemented with 10% FBS and 1% penicillin-streptomycin. All the cells were cultured in an incubator under a humid atmosphere with 5% CO_2 at 37°C.

Isolation of tissue-derived mitoEVs

Tissue-derived EVs were isolated from mouse skeletal muscle tissues according to previously reported methods with optimization (*22*). To obtain enough skeletal muscle tissue for EV isolation and considering the accessibility of the skeletal muscles, the major muscle groups of the mouse hind limb, including the tibialis anterior (TA), soleus, and gastrocnemius muscles, were collected for EV isolation. In brief, skeletal muscle was dissected from euthanized mice, cut into 1- to 3-mm^3 pieces and washed with phosphate-buffered saline (PBS). Then, the muscle pieces were digested with collagenase IV (1 mg/ml; 17104019, Gibco) and dispase (1 U/ml; D6430, Solarbio, Beijing, China) in a shaking incubator at 37°C for 2 hours. After digestion, a large volume of precooled DMEM was used for neutralization, followed by centrifugation at 300*g* for 10 min to remove tissue masses and 2000*g* for 40 min at 4°C to remove cells and other debris. The supernatant was subsequently ultracentrifuged at 30,000*g* for 60 min at 4°C in an SW32Ti rotor (Beckman Coulter, Brea, CA, USA) to obtain mitoEVs and further ultracentrifuged at 110,000*g* for 70 min at 4°C to obtain non-mitoEVs. All EVs were washed with PBS and then subjected to a second UC step at either 30,000*g* or 110,000*g*.

For the conventional isolation method (*56*), muscle pieces were incubated in a suspension culture bottle for 24 hours at 37°C under 5% CO_2. Afterward, the supernatant was collected, and the differential UC procedure mentioned above was performed to obtain EVs. Last, the purified EVs were resuspended in sterile PBS and stored at −80°C until further use.

Transmission electron microscopy

The morphology of EVs or muscle tissues was observed using TEM (HT7800, Hitachi Ltd., Tokyo, Japan) as previously described (*22*, *57*). For observation of EV samples, the EV suspension was dropped on a carbon-coated copper grid, followed by washing with pure water to remove unattached EVs. The grid was then stained with 2% phosphotungstic acid and air dried before being subjected to TEM. For the preparation of tissue TEM samples, normal and postexercise muscle tissues were quickly fixed at 4°C in 3% glutaraldehyde and postfixed in 1% osmium tetroxide, followed by tissue dehydration and resin embedding. The embedded tissues were subsequently cut into ultrathin sections (70 nm), stained with 2% uranyl acetate and Reynolds lead citrate, and then observed via TEM.

Nanoparticle tracking analysis

The size distribution and particle number of the EVs were analyzed using a Zeta View PMX 120 (Particle Metrix, Meerbusch, Germany) as previously described (*57*). In brief, EVs were diluted with pure water and analyzed via the following parameters (Max Area 1000, Min Area 5, and Min Brightness 20) at 25°C.

Western blotting

EV protein was extracted using radioimmunoprecipitation assay buffer (Beyotime) containing protease inhibitors (Calbiochem, San Diego, CA, USA). The protein concentration was determined using a BCA protein assay kit (Thermo Fisher Scientific, Carlsbad, CA, USA). Equal particle numbers of EVs or equal amounts of EV protein were electrophoresed using sodium dodecyl sulfate–polyacrylamide gels, and then transferred to nitrocellulose membranes (Cytiva, Germany). The membranes were blocked in western blocking buffer (P0252, Beyotime) and incubated with anti-GM130 (A11408, ABClonal, Wuhan, China), anti-HSP70 (A0284, ABClonal), anti-TSG101 (14497-1-AP, Proteintech, Wuhan, China), anti-COXIV (11242-1-AP, Proteintech), anti-ATP5a (A5884, ABClonal), anti-VDAC (55259-1-AP, Proteintech), anti-TOM20 (no. 42406, Cell Signaling Technology, Beverly, MA, USA), anti-PDHB (14744-1-AP, Proteintech), and anti-pyruvate carboxylase (PC, 16588-1-AP, Proteintech) at 4°C overnight. Afterward, the membranes were washed and incubated with horseradish peroxidase–conjugated secondary antibodies at 37°C for 1 hour. The protein bands were detected using a chemiluminescence kit (MedChem Express, Shanghai, China) and analyzed using ImageJ software (National Institutes of Health, Bethesda, MD, USA).

Quantitative real-time PCR

Total RNA was extracted from tissues or cells using TRIzol reagent (Gibco) and reverse transcribed into cDNA via a commercial kit (Vazyme, Nanjing, China). Quantitative real-time PCR (qPCR) was carried out on a CFX96 real-time PCR detection system (Bio-Rad, Hercules, CA, USA) using SYBR Green (Vazyme). The primer sequences are available in table S1. Human *RPS18* and murine *Rps18* served as internal controls.

Detection of mtDNA expression

Total DNA was extracted from EVs or cells using a Universal Genomic DNA Kit (CwBio, Taizhou, China). The relative mtDNA copy numbers were determined by qPCR analysis, in which murine *CoxII* and human *ND1* were used as target mitochondrial genes and the nuclear gene *Rps18* was used as a normalization control. For long-range PCR, the DNA templates of EVs (10 ng) were amplified using G5 High-Fidelity DNA Polymerase (EnzyArtisan, Shanghai, China) at an annealing temperature of 68°C (for LRP1) or 60°C (for LRP2). The PCR products were visualized by 0.8% agarose gel electrophoresis. For standard PCR, the DNA templates of EVs (10 ng) and cells (400 ng) were amplified at an annealing temperature of 60°C according to the 2 × Taq Master Mix (Vazyme) instructions. The PCR products were electrophoresed via a 1% agarose gel and visualized using a Tanon 3500BR Gel Image System (Tanon). All primer sequences are provided in tables S2 and S3.

Mouse acute exercise model

C57BL/6 mice were subjected to exercise regimens (HIIT) on a treadmill following previously reported methods with some modifications (*58*). In brief, the HIIT group began with a warm-up for 10 min at a speed of 6 m/min. This was followed by six rounds of alternating training at low intensity (8 m/min, 5 min), medium intensity (16 m/min, 8 min), and complete rest (0 m/min, 2 min). Subsequently, another six rounds of alternating training were performed, consisting of low intensity (8 m/min, 2 min), high intensity (24 m/min, 4 min), and complete rest (0 m/min, 1 min). After HIIT, all the mice were euthanized for the collection of skeletal muscle samples.

RNA-seq analysis of tissue samples

After different treatments, mouse muscle or kidney tissues were collected for RNA-seq analysis. In brief, total RNA of tissue samples was extracted using TRIzol and then treated with deoxyribonuclease I (Takara, Shiga, Japan) to remove genomic DNA. The RNA-seq transcriptome library was constructed using a TruSeq RNA Sample Preparation Kit (Illumina, San Diego, CA, USA), and the paired-end RNA-seq sequencing library was sequenced on an Illumina HiSeq xten/NovaSeq 6000 sequencer by Shanghai Majorbio Biopharm Technology Co. Ltd. (Shanghai, China). The DEGs with a FC > 1.5 and *P*-adjusted < 0.05 were considered significant. The PCA plot, volcano plot, and heatmap were generated using a free online platform (https://omicsolution.com/wkomics/wkold/). GO analysis of the DEGs was performed using STRING (https://cn.string-db.org/) and visualized using Cytoscape software (version 3.7.2), and a false discovery rate (FDR) < 0.05 was considered to indicate statistical significance.

Proteomic analysis of tissue EVs

Total protein was extracted from EV samples using a protein lysis buffer (8 M urea and 1% SDS) and quantified with a BCA kit (Thermo Fisher Scientific). EV protein samples (100 μg) were taken for reductive alkylation and digested with trypsin overnight at 37°C. The trypsin-digested peptides were desalted and drained with a vacuum concentrator. Then, the peptides were analyzed using a VanquishNeo coupled with an Orbitrap Astral mass spectrometer (Thermo Fisher Scientific) at Majorbio Bio-Pharm Technology Co. Ltd. (Shanghai, China). In brief, the peptides were dissolved in 0.1% formic acid and separated on an ES906 column (150 μm × 15 cm, Thermo Fisher Scientific) over a 60 SPD gradient at a flow rate of 500 nl/min. Data-independent acquisition data were acquired using an Orbitrap Astral mass spectrometer, with MS data were collected over a mass/charge ratio range of 100 to 1700. Bioinformatic analysis of the proteomic data was performed with the Majorbio Cloud platform (https://cloud.majorbio.com). DEPs were identified using thresholds of FC > 2 and *P*-adjusted <0.05. PCA plots, volcano plots, and heatmaps were generated using a free online platform (https://omicsolution.com/wkomics/wkold/). GO analysis of the DEPs was performed using STRING (https://cn.string-db.org/), with FDR < 0.05 considered significant. The proteomics data of mitoEVs were compared with those of established EV proteomics databases, including Vesiclepedia (http://microvesicles.org/) and Exocarta (http://www.exocarta.org/).

Polarized mitochondria measurement

The MMP of the EV samples was evaluated using MitoTracker Deep Red Probes (Thermo Fisher Scientific). In brief, the dye was diluted in 0.22-μm filtered PBS to a final concentration of 400 nM and subjected to UC at 110,000*g* for 60 min at 4°C to remove the aggregated dye. The free dye was then resuspended in 0.22-μm filtered PBS to label the EVs (2 μg in 100 μl) at 37°C for 30 min in the dark. The MMP of the labeled EVs was detected using the Cytek Aurora spectral flow

cytometer (Cytekbio, Shanghai, China) with excitation at 644 nm and emission at 665 nm.

Mitochondrial ROS measurement

The levels of mitochondrial ROS in EV samples were analyzed using the MitoSOX Red mitochondrial superoxide indicator (MitoSOX, Thermo Fisher Scientific). In brief, free dye (10 μM) obtained by UC (with the aim of removing aggregated dye) was used to label EVs (2 μg in 100 μl) at 37°C for 15 min in the dark. The mitochondrial ROS of the labeled EVs were detected via a Cytek Aurora spectral flow cytometer (Cytekbio) with excitation at 510 nm and emission at 580 nm.

For total intracellular ROS measurement, a 2′,7′-Dichlorodihydrofluorescein diacetate (DCFH-DA) superoxide indicator (Beyotime Biotechnology, Shanghai, China) was used according to the manufacturer's instructions. After different treatments, the cells were stained with DCFH-DA (10 μM) at 37°C for 20 min in the dark, and the fluorescence was detected via a flow cytometer (CytoFLUX, Chengdu, China).

Mitochondrial respiratory capacity assays

The bioenergetic profile of HK-2 cells was assessed using the Seahorse XF Flux Analyzer (Seahorse Biosciences, Agilent, USA) according to the manufacturer's instructions. HK-2 cells were seeded at a density of 40,000 cells per well (for the XF24 analyzer) or 8000 cells per well (for the XF96 Pro analyzer) in cell culture microplates. After 24 hours of treatment with different EVs (4×10^9 particles/ml), the culture medium of HK-2 cells was replaced with complete Seahorse XF DMEM medium. Following equilibration, the cells were sequentially treated with oligomycin (1 μM), carbonyl cyanide ptrifluoromethoxyphenylhydrazone (FCCP; 1 μM), and rotenone-antimycin (0.5 μM) to measure the oxygen consumption rate. On the day of the assay, each well on the plate was verified to be subconfluent with comparable cell density, and the results were normalized to cell number. For the H_2O_2-induced oxidative stress model, HK-2 cells were pretreated with EVs (2×10^{10} particles/ml) for 2 hours, followed by the addition of H_2O_2 (100 μM) to induce cellular damage. After 24 hours of treatment, HK-2 cells were seeded at 8000 cells per well in an XF96 Seahorse microplate. After 4 hours, the medium was replaced with complete Seahorse XF DMEM medium, and the cells were sequentially treated with oligomycin (1 μM), FCCP (1 μM), and rotenone-antimycin (0.5 μM) to assess mitochondrial activity. The data were analyzed using Agilent Seahorse XF Wave Pro software (version 10).

Intracellular EV tracking assay

Tissue EVs (2×10^9 particles) were labeled with PKH26 (10 μM, Sigma-Aldrich, St. Louis, MO, USA) according to the manufacturer's protocols, and EV-DNA was labeled with ethidium bromide–*N*,*N*′-bisacrylamide (EtBr; 2 μg/ml). HK-2 cells were incubated with dye-labeled EVs for 8 hours at 37°C. After being washed with PBS, the cells were stained with MitoTracker Green Probes (200 nM, Thermo Fisher Scientific) to label the mitochondria and with Hoechst 33342 Staining Solution for Live Cells (Beyotime) to label the nuclei at 37°C for 30 min. The mitochondria (magenta), internalized EVs (green), EV-DNA (yellow), and nuclei (blue) were observed using SpinSR spinning disk confocal super resolution microscope (Olympus) and analyzed with OlyVIA 3.3 software (Olympus).

Size exclusion chromatography

In accordance with the MISEV2018 guidelines (*52*), the SEC protocol is recommended as a method with high specificity for EVs isolation and purification. Thus, a commercial SEC kit (Exosupur, Echo Biotech, Beijing, China) was used to purify EVs according to the manufacturer's instructions. In brief, the EV samples obtained via the UC method were loaded onto the SEC column, and the fractions were eluted by the continuous addition of filtered PBS. A total of 16 or 24 elution fractions were collected. Each fraction was analyzed for particle concentration using nanoparticle tracking analysis and for protein concentration using a Micro BCA assay (Thermo Fisher Scientific). Values below the detection limit were considered as zero. All collected fractions were stored at −80°C for further analyses.

High-resolution flow cytometry analysis

The isolated EVs were labeled with CFSE (Thermo Fisher Scientific) as previously reported (*27*, *28*). In brief, EVs (4×10^9 particles in 100 μl) diluted in 0.22-μm filtered PBS were incubated with CFSE (40 μM) at 37°C for 30 min. The CFSE-labeled EVs were analyzed using a high-resolution flow cytometer (Cytek Aurora spectral, Cytekbio) with excitation at 492 nm and emission at 517 nm. Negative controls, including PBS, unstained EVs, and dye alone, were used to eliminate nonspecific fluorescence. To assess the integrity of the EVs, the stained EVs were lysed via incubation with detergent Triton X-100 [final concentration at 1% (v/v), LABLEAD, Beijing, China] at room temperature for 30 min as previously reported (*27*). The fluorescence of the lysed EVs was analyzed using an Cytek Aurora spectral flow cytometer (Cytekbio). All flow cytometry data were analyzed with FlowJo (version 10).

Mouse acute muscle injury model and treatments

C57BL/6 mice were randomly divided into four groups ($n = 6$): the healthy control group (Con), acute muscle injury (AMI) group, AMI + mitoEV group, and AMI + non-mitoEV group. To establish a mouse model of AMI, cardiotoxin (25 μl of 20 μM, Sigma-Aldrich) was i.m. injected into the TA muscle. One hour after cardiotoxin injection, 25 μl of PBS or EVs (~5×10^{10} particles per TA) were administered by i.m. injection into the TA muscle of each mouse. Three days after EV treatment, all the mice were euthanized by an overdose of anesthesia, and muscle samples were collected for further analysis.

Histological examination

Muscle or kidney samples of mice were fixed in 4% paraformaldehyde, dehydrated in an ethanol gradient, and embedded in paraffin. Subsequently, the samples were sliced into 4-μm-thick sections, followed by hematoxylin and eosin (H&E), Masson's trichrome, and immunohistochemistry (IHC) staining. For IHC staining, tissue sections were stained with primary antibodies including anti-F4/80 (#70076, Cell Signaling Technology), anti-ICAM (10831-1-AP, Proteintech), anti-TOM20 (#42406, Cell Signaling Technology), anti-CD68 (BA3638, BOSTER, Wuhan, China), and anti-TFAM (22586-1-AP, Proteintech), and scanned using a digital pathology section scanner (NanoZoomer S360, Hamamatsu Photonics, Japan) and quantified using ImageJ.

In vivo biodistribution of EVs in mice

MitoEVs or non-mitoEVs were labeled with sulfo-Cy7-NHS ester according to the manufacturer's instructions (New Research Biosciences Co. Ltd., Xi'an, China). Cy7-labeled mitoEVs and non-mitoEVs (Cy7-EVs, ~1×10^{11} particles in 100 μl of PBS per mouse) were i.p. injected into C57BL/6 mice. At 4 hours after injection, the mice were euthanized by an overdose of pentobarbital sodium anesthesia,

and the organs, including the hearts, lungs, livers, kidneys and spleens, were collected and observed on a multimodel in vivo animal imaging system (Biolight, Guangzhou, China).

Mouse CKD model and treatments

C57BL/6 mice were randomly divided into four groups ($n = 6$): the healthy control group (Con), CKD group, CKD + mitoEV group, and CKD + non-mitoEV group. A mouse model of CKD was induced by i.p. injection of folic acid (250 mg/kg, Sigma-Aldrich), and PBS or EVs were administered via i.p. injection on days 0, 2, 4, and 6 after modeling. The dosage of EVs administered each time was ~1×10^{11} particles per mouse. On day 14 after EV treatment, all mice were euthanized by an overdose of anesthesia, and kidney samples were collected for further analysis.

Detection of tissue cell uptake of mitoEVs in vivo

The mitoEVs were labeled with DiD dye (5 μM, Thermo Fisher Scientific) and further purified via UC according to manufacturer's instructions. The purified DiD-labeled mitoEVs (5×10^{10} for AMI mice and 1×10^{11} for CKD mice) were administered via i.m. injection to AMI mice and i.p. injection into CKD mice. Then, mouse muscle and kidney tissues were collected at 2 hours postinjection and sliced for microscopic-level observation. For IF staining, muscle tissue sections were stained with anti-laminin (ab11575, Abcam) to localize myofibers and with anti-Ly6C (GB115601, Servicebio, Wuhan, China) to indicate monocytes. Kidney tissue sections were stained with anti-AQP1 (ab9566, Abcam) to mark renal tubular cells and with anti-Ly6C (GB115601, Servicebio) to indicate monocytes. The stained tissue sections were observed using a SpinSR spinning disk confocal super resolution microscope (Olympus) and analyzed with OlyVIA 3.3 software (Olympus).

Statistical analysis

All the data are presented as the means ± standard deviations and were analyzed using GraphPad software (version 8.0.2, IBM Corporation, USA) with t tests (for two-group comparisons) or one-way analysis of variance (ANOVA) (for more than two group comparisons), and $P < 0.05$ was considered to indicate a significant difference. The data were obtained from at least three biological replicates, and "n" represents the number of independent samples for each group.

Supplementary Materials

This PDF file includes:

Figs. S1 to S21
Tables S1 to S3
Uncropped Western blots

REFERENCES AND NOTES

1. A. S. Monzel, J. A. Enríquez, M. Picard, Multifaceted mitochondria: Moving mitochondrial science beyond function and dysfunction. *Nat. Metab.* **5**, 546–562 (2023).
2. M. P. Murphy, R. C. Hartley, Mitochondria as a therapeutic target for common pathologies. *Nat. Rev. Drug Discov.* **17**, 865–886 (2018).
3. F. Emma, G. Montini, S. M. Parikh, L. Salviati, Mitochondrial dysfunction in inherited renal disease and acute kidney injury. *Nat. Rev. Nephrol.* **12**, 267–280 (2016).
4. S. Ranjbarvaziri, K. B. Kooiker, M. Ellenberger, G. Fajardo, M. Zhao, A. S. Vander Roest, R. A. Woldeyes, T. T. Koyano, R. Fong, N. Ma, L. Tian, G. M. Traber, F. Chan, J. Perrino, S. Reddy, W. Chiu, J. C. Wu, J. Y. Woo, K. M. Ruppel, J. A. Spudich, M. P. Snyder, K. Contrepois, D. Bernstein, Altered cardiac energetics and mitochondrial dysfunction in hypertrophic cardiomyopathy. *Circulation* **144**, 1714–1731 (2021).
5. T. Mito, A. E. Vincent, J. Faitg, R. W. Taylor, N. A. Khan, T. G. McWilliams, A. Suomalainen, Mosaic dysfunction of mitophagy in mitochondrial muscle disease. *Cell Metab.* **34**, 197–208.e5 (2022).
6. A. Diaz-Vegas, P. Sanchez-Aguilera, J. R. Krycer, P. E. Morales, M. Monsalves-Alvarez, M. Cifuentes, B. A. Rothermel, S. Lavandero, Is mitochondrial dysfunction a common root of noncommunicable chronic diseases? *Endocr. Rev.* **41**, bnaa005 (2020).
7. C. Tang, J. Cai, X. M. Yin, J. M. Weinberg, M. A. Venkatachalam, Z. Dong, Mitochondrial quality control in kidney injury and repair. *Nat. Rev. Nephrol.* **17**, 299–318 (2021).
8. T. Huang, T. Zhang, J. Gao, Targeted mitochondrial delivery: A therapeutic new era for disease treatment. *J. Control. Release* **343**, 89–106 (2022).
9. P. Lou, S. Liu, X. Xu, C. Pan, Y. Lu, J. Liu, Extracellular vesicle-based therapeutics for the regeneration of chronic wounds: Current knowledge and future perspectives. *Acta Biomater.* **119**, 42–56 (2021).
10. X. Zhou, S. Liu, Y. Lu, M. Wan, J. Cheng, J. Liu, MitoEVs: A new player in multiple disease pathology and treatment. *J Extracell. Vesicles* **12**, e12320 (2023).
11. P. D'Acunzo, R. Pérez-González, Y. Kim, T. Hargash, C. Miller, M. J. Alldred, H. Erdjument-Bromage, S. C. Penikalapati, M. Pawlik, M. Saito, M. Saito, S. D. Ginsberg, T. A. Neubert, C. N. Goulbourne, E. Levy, Mitovesicles are a novel population of extracellular vesicles of mitochondrial origin altered in Down syndrome. *Sci. Adv.* **7**, eabe5085 (2021).
12. W. Liang, S. Sagar, R. Ravindran, R. H. Najor, J. M. Quiles, L. Chi, R. Y. Diao, B. P. Woodall, L. J. Leon, E. Zumaya, J. Duran, D. M. Cauvi, A. De Maio, E. D. Adler, Å. B. Gustafsson, Mitochondria are secreted in extracellular vesicles when lysosomal function is impaired. *Nat. Commun.* **14**, 5031 (2023).
13. D. S. Manickam, Delivery of mitochondria via extracellular vesicles – A new horizon in drug delivery. *J. Control. Release* **343**, 400–407 (2022).
14. N. Borcherding, J. R. Brestoff, The power and potential of mitochondria transfer. *Nature* **623**, 283–291 (2023).
15. G. Ikeda, M. R. Santoso, Y. Tada, A. M. Li, E. Vaskova, J.-H. Jung, C. O'Brien, E. Egan, J. Ye, P. C. Yang, Mitochondria-rich extracellular vesicles from autologous stem cell-derived cardiomyocytes restore energetics of ischemic myocardium. *J. Am. Coll. Cardiol.* **77**, 1073–1088 (2021).
16. K. M. Dave, D. B. Stolz, D. S. Manickam, Delivery of mitochondria-containing extracellular vesicles to the BBB for ischemic stroke therapy. *Expert Opin. Drug Deliv.* **20**, 1769–1788 (2023).
17. K. M. Dave, D. B. Stolz, V. R. Venna, V. A. Quaicoe, M. E. Maniskas, M. J. Reynolds, R. Babidhan, D. X. Dobbins, M. N. Farinelli, A. Sullivan, T. N. Bhatia, H. Yankello, R. Reddy, Y. Bae, R. K. Leak, S. S. Shiva, L. D. McCullough, D. S. Manickam, Mitochondria-containing extracellular vesicles (EV) reduce mouse brain infarct sizes and EV/HSP27 protect ischemic brain endothelial cultures. *J. Control. Release* **354**, 368–393 (2023).
18. K. M. Dave, V. R. Venna, K. S. Rao, D. B. Stolz, B. Brady, V. A. Quaicoe, M. E. Maniskas, E. E. Hildebrand, D. Green, M. Chen, J. Milosevic, S.-y. Zheng, S. S. Shiva, L. D. McCullough, D. S. Manickam, Mitochondria-containing extracellular vesicles from mouse vs. human brain endothelial cells for ischemic stroke therapy. *J. Control. Release* **373**, 803–822 (2024).
19. A. D'Souza, A. Burch, K. M. Dave, A. Sreeram, M. J. Reynolds, D. X. Dobbins, Y. S. Kamte, W. Zhao, C. Sabatelle, G. M. Joy, V. Soman, U. R. Chandran, S. S. Shiva, N. Quillinan, P. S. Herson, D. S. Manickam, Microvesicles transfer mitochondria and increase mitochondrial function in brain endothelial cells. *J. Control. Release* **338**, 505–526 (2021).
20. K. Hayakawa, E. Esposito, X. Wang, Y. Terasaki, Y. Liu, C. Xing, X. Ji, E. H. Lo, Transfer of mitochondria from astrocytes to neurons after stroke. *Nature* **535**, 551–555 (2016).
21. M. Zhao, S. Liu, C. Wang, Y. Wang, M. Wan, F. Liu, M. Gong, Y. Yuan, Y. Chen, J. Cheng, Y. Lu, J. Liu, Mesenchymal stem cell-derived extracellular vesicles attenuate mitochondrial damage and inflammation by stabilizing mitochondrial DNA. *ACS Nano* **15**, 1519–1538 (2021).
22. P. Lou, S. Liu, Y. Wang, K. Lv, X. Zhou, L. Li, Y. Zhang, Y. Chen, J. Cheng, Y. Lu, J. Liu, Neonatal-tissue-derived extracellular vesicle therapy (NEXT): A potent strategy for precision regenerative medicine. *Adv. Mater.* **35**, e2300602 (2023).
23. S. Larsen, J. Nielsen, C. N. Hansen, L. B. Nielsen, F. Wibrand, N. Stride, H. D. Schroder, R. Boushel, J. W. Helge, F. Dela, M. Hey-Mogensen, Biomarkers of mitochondrial content in skeletal muscle of healthy young human subjects. *J. Physiol.* **590**, 3349–3360 (2012).
24. Y. Lei, M. Gan, Y. Qiu, Q. Chen, X. Wang, T. Liao, M. Zhao, L. Chen, S. Zhang, Y. Zhao, L. Niu, Y. Wang, L. Zhu, L. Shen, The role of mitochondrial dynamics and mitophagy in skeletal muscle atrophy: From molecular mechanisms to therapeutic insights. *Cell. Mol. Biol. Lett.* **29**, 59 (2024).
25. P. D'Acunzo, Y. Kim, J. M. Ungania, R. Pérez-González, C. N. Goulbourne, E. Levy, Isolation of mitochondria-derived mitovesicles and subpopulations of microvesicles and exosomes from brain tissues. *Nat. Protoc.* **17**, 2517–2549 (2022).
26. K. P. De Sousa, I. Rossi, M. Abdullahi, M. I. Ramirez, D. Stratton, J. M. Inal, Isolation and characterization of extracellular vesicles and future directions in diagnosis and therapy. *Wiley Interdiscip. Rev. Nanomed. Nanobiotechnol.* **15**, e1835 (2023).
27. F. Ender, P. Zamzow, N. V. Bubnoff, F. Gieseler, Detection and quantification of extracellular vesicles via FACS: Membrane labeling matters! *Int. J. Mol. Sci.* **21**, 291 (2020).
28. A. Morales-Kastresana, B. Telford, T. A. Musich, K. McKinnon, C. Clayborne, Z. Braig, A. Rosner, T. Demberg, D. C. Watson, T. S. Karpova, G. J. Freeman, R. H. DeKruyff,

G. N. Pavlakis, M. Terabe, M. Robert-Guroff, J. A. Berzofsky, J. C. Jones, Labeling extracellular vesicles for nanoscale flow cytometry. *Sci. Rep.* **7**, 1878 (2017).
29. M. Yáñez-Mó, P. R.-M. Siljander, Z. Andreu, A. B. Zavec, F. E. Borràs, E. I. Buzas, K. Buzas, E. Casal, F. Cappello, J. Carvalho, E. Colás, A. Cordeiro-da Silva, S. Fais, J. M. Falcon-Perez, I. M. Ghobrial, B. Giebel, M. Gimona, M. Graner, I. Gursel, M. Gursel, N. H. H. Heegaard, A. Hendrix, P. Kierulf, K. Kokubun, M. Kosanovic, V. Kralj-Iglic, E. M. Krämer-Albers, S. Laitinen, C. Lässer, T. Lener, E. Ligeti, A. Linē, G. Lipps, A. Llorente, J. Lötvall, M. Manček-Keber, A. Marcilla, M. Mittelbrunn, I. Nazarenko, E. N. M. Nolte-'t Hoen, T. A. Nyman, L. O'Driscoll, M. Olivan, C. Oliveira, É. Pállinger, H. A. Del Portillo, J. Reventós, M. Rigau, E. Rohde, M. Sammar, F. Sánchez-Madrid, N. Santarém, K. Schallmoser, M. S. Ostenfeld, W. Stoorvogel, R. Stukelj, S. G. Van der Grein, M. H. Vasconcelos, M. H. M. Wauben, O. De Wever, Biological properties of extracellular vesicles and their physiological functions. *J. Extracell. Vesicles* **4**, 27066 (2015).
30. N. Pfanner, B. Warscheid, N. Wiedemann, Mitochondrial proteins: From biogenesis to functional networks. *Nat. Rev. Mol. Cell Biol.* **20**, 267–284 (2019).
31. W. T. Lee, X. Sun, T. S. Tsai, J. L. Johnson, J. A. Gould, D. J. Garama, D. J. Gough, M. McKenzie, I. A. Trounce, J. C. St. John, Mitochondrial DNA haplotypes induce differential patterns of DNA methylation that result in differential chromosomal gene expression patterns. *Cell Death Discov.* **3**, 17062 (2017).
32. B. Guan, Y. Liu, B. Xie, S. Zhao, A. Yalikun, W. Chen, M. Zhou, Q. Gu, D. Yan, Mitochondrial genome transfer drives metabolic reprogramming in adjacent colonic epithelial cells promoting TGFβ1-mediated tumor progression. *Nat. Commun.* **15**, 3653 (2024).
33. D. J. Walsh, D. J. Bernard, F. Pangilinan, M. Esposito, D. Harold, A. Parle-McDermott, L. C. Brody, Mito-SiPE is a sequence-independent and PCR-free mtDNA enrichment method for accurate ultra-deep mitochondrial sequencing. *Commun. Biol.* **5**, 1269 (2022).
34. A. J. Kowaltowski, F. Abdulkader, How and when to measure mitochondrial inner membrane potentials. *Biophys. J.* **123**, 4150–4157 (2024).
35. R. Hazan Ben-Menachem, D. Lintzer, T. Ziv, K. Das, I. Rosenhek-Goldian, Z. Porat, H. Ben Ami Pilo, S. Karniely, A. Saada, N. Regev-Rudzki, O. Pines, Mitochondrial-derived vesicles retain membrane potential and contain a functional ATP synthase. *EMBO Rep.* **24**, e56114 (2023).
36. M. N. Islam, S. R. Das, M. T. Emin, M. Wei, L. Sun, K. Westphalen, D. J. Rowlands, S. K. Quadri, S. Bhattacharya, J. Bhattacharya, Mitochondrial transfer from bone-marrow-derived stromal cells to pulmonary alveoli protects against acute lung injury. *Nat. Med.* **18**, 759–765 (2012).
37. R. Z. Lin, G. B. Im, A. C. Luo, Y. Zhu, X. Hong, J. Neumeyer, H. W. Tang, N. Perrimon, J. M. Melero-Martin, Mitochondrial transfer mediates endothelial cell engraftment through mitophagy. *Nature* **629**, 660–668 (2024).
38. W. Chen, H. Zhao, Y. Li, Mitochondrial dynamics in health and disease: Mechanisms and potential targets. *Signal Transduct. Target. Ther.* **8**, 333 (2023).
39. I. Garcia, E. Jones, M. Ramos, W. Innis-Whitehouse, R. Gilkerson, The little big genome: The organization of mitochondrial DNA. *Front. Biosci. (Landmark Ed)* **22**, 710–721 (2017).
40. J. Guo, C. Wu, X. Lin, J. Zhou, J. Zhang, W. Zheng, T. Wang, Y. Cui, Establishment of a simplified dichotomic size-exclusion chromatography for isolating extracellular vesicles toward clinical applications. *J. Extracell. Vesicles* **10**, e12145 (2021).
41. A. E. Qualls, W. M. Southern, J. A. Call, Mitochondria-cytokine crosstalk following skeletal muscle injury and disuse: A mini-review. *Am. J. Physiol. Cell Physiol.* **320**, C681–C688 (2021).
42. P. Bhargava, R. G. Schnellmann, Mitochondrial energetics in the kidney. *Nat. Rev. Nephrol.* **13**, 629–646 (2017).
43. D. L. Galvan, N. H. Green, F. R. Danesh, The hallmarks of mitochondrial dysfunction in chronic kidney disease. *Kidney Int.* **92**, 1051–1057 (2017).
44. N. M. Selby, M. W. Taal, What every clinician needs to know about chronic kidney disease: Detection, classification and epidemiology. *Diabetes Obes. Metab.* **26**, 3–12 (2024).
45. J. R. Melamed, S. S. Yerneni, M. L. Arral, S. T. LoPresti, N. Chaudhary, A. Sehrawat, H. Muramatsu, M. G. Alameh, N. Pardi, D. Weissman, G. K. Gittes, K. A. Whitehead, Ionizable lipid nanoparticles deliver mRNA to pancreatic β cells via macrophage-mediated gene transfer. *Sci. Adv.* **9**, eade1444 (2023).
46. Z. Gan, T. Fu, D. P. Kelly, R. B. Vega, Skeletal muscle mitochondrial remodeling in exercise and diseases. *Cell Res.* **28**, 969–980 (2018).
47. M. Whitham, B. L. Parker, M. Friedrichsen, J. R. Hingst, M. Hjorth, W. E. Hughes, C. L. Egan, L. Cron, K. I. Watt, R. P. Kuchel, N. Jayasooriah, E. Estevez, T. Petzold, C. M. Suter, P. Gregorevic, B. Kiens, E. A. Richter, D. E. James, J. F. P. Wojtaszewski, M. A. Febbraio, Extracellular vesicles provide a means for tissue crosstalk during exercise. *Cell Metab.* **27**, 237–251.e4 (2018).
48. D. A. Hood, J. M. Memme, A. N. Oliveira, M. Triolo, Maintenance of skeletal muscle mitochondria in health, exercise, and aging. *Annu. Rev. Physiol.* **81**, 19–41 (2019).
49. A. N. Oliveira, B. J. Richards, M. Slavin, D. A. Hood, Exercise is muscle mitochondrial medicine. *Exerc. Sport Sci. Rev.* **49**, 67–76 (2021).
50. R. N. Lightowlers, Z. M. Chrzanowska-Lightowlers, O. M. Russell, Mitochondrial transplantation-a possible therapeutic for mitochondrial dysfunction?: Mitochondrial transfer is a potential cure for many diseases but proof of efficacy and safety is still lacking. *EMBO Rep.* **21**, e50964 (2020).
51. J. C. Lee, R. M. Ray, T. A. Scott, Prospects and challenges of tissue-derived extracellular vesicles. *Mol. Ther.* **32**, 2950–2978 (2024).
52. C. Théry, K. W. Witwer, E. Aikawa, M. J. Alcaraz, J. D. Anderson, R. Andriantsitohaina, A. Antoniou, T. Arab, F. Archer, G. K. Atkin-Smith, D. C. Ayre, J.-M. Bach, D. Bachurski, H. Baharvand, L. Balaj, S. Baldacchino, N. N. Bauer, A. A. Baxter, M. Bebawy, C. Beckham, A. B. Zavec, A. Benmoussa, A. C. Berardi, P. Bergese, E. Bielska, C. Blenkiron, S. Bobis-Wozowicz, E. Boilard, W. Boireau, A. Bongiovanni, F. E. Borràs, S. Bosch, C. M. Boulanger, X. Breakefield, A. M. Breglio, M. Á. Brennan, D. R. Brigstock, A. Brisson, M. L. Broekman, J. F. Bromberg, P. Bryl-Górecka, S. Buch, A. H. Buck, D. Burger, S. Busatto, D. Buschmann, B. Bussolati, E. I. Buzás, J. B. Byrd, G. Camussi, D. R. Carter, S. Caruso, L. W. Chamley, Y.-T. Chang, C. Chen, S. Chen, L. Cheng, A. R. Chin, A. Clayton, S. P. Clerici, A. Cocks, E. Cocucci, R. J. Coffey, A. Cordeiro-da-Silva, Y. Couch, F. A. Coumans, B. Coyle, R. Crescitelli, M. F. Criado, C. D'Souza-Schorey, S. Das, A. D. Chaudhuri, P. de Candia, E. F. De Santana, O. De Wever, H. A. Del Portillo, T. Demaret, S. Deville, A. Devitt, B. Dhondt, D. D. Vizio, L. C. Dieterich, V. Dolo, A. P. Dominguez Rubio, M. Dominici, M. R. Dourado, T. A. Driedonks, F. V. Duarte, H. M. Duncan, R. M. Eichenberger, K. Ekström, S. E. Andaloussi, C. Elie-Caille, U. Erdbrügger, J. M. Falcón-Pérez, F. Fatima, J. E. Fish, M. Flores-Bellver, A. Försönits, A. Frelet-Barrand, F. Fricke, G. Fuhrmann, S. Gabrielsson, A. Gámez-Valero, C. Gardiner, K. Gärtner, R. Gaudin, Y. S. Gho, B. Giebel, C. Gilbert, M. Gimona, I. Giusti, D. C. Goberdhan, A. Görgens, S. M. Gorski, D. W. Greening, J. C. Gross, A. Gualerzi, G. N. Gupta, D. Gustafson, A. Handberg, R. A. Haraszti, P. Harrison, H. Hegyesi, A. Hendrix, A. F. Hill, F. H. Hochberg, K. F. Hoffmann, B. Holder, H. Holthofer, B. Hosseinkhani, G. Hu, Y. Huang, V. Huber, S. Hunt, A. G.-E. Ibrahim, T. Ikezu, J. M. Inal, M. Isin, A. Ivanova, H. K. Jackson, S. Jacobsen, S. M. Jay, M. Jayachandran, G. Jenster, L. Jiang, S. M. Johnson, J. C. Jones, A. Jong, T. Jovanovic-Talisman, S. Jung, R. Kalluri, S.-I. Kano, S. Kaur, Y. Kawamura, E. T. Keller, D. Khamari, E. Khomyakova, A. Khvorova, P. Kierulf, K. P. Kim, T. Kislinger, M. Klingeborn, D. J. Klinke II, M. Kornek, M. M. Kosanović, Á. F. Kovács, E.-M. Krämer-Albers, S. Krasemann, M. Krause, I. V. Kurochkin, G. D. Kusuma, S. Kuypers, S. Laitinen, S. M. Langevin, L. R. Languino, J. Lannigan, C. Lässer, L. C. Laurent, G. Lavieu, E. Lázaro-Ibáñez, S. L. Lay, M.-S. Lee, Y. X. F. Lee, D. S. Lemos, M. Lenassi, A. Leszczynska, I. T. Li, K. Liao, S. F. Libregts, E. Ligeti, R. Lim, S. K. Lim, A. Linē, K. Linnemannstöns, A. Llorente, C. A. Lombard, M. J. Lorenowicz, Á. M. Lörincz, J. Lötvall, J. Lovett, M. C. Lowry, X. Loyer, Q. Lu, B. Lukomska, T. R. Lunavat, S. L. Maas, H. Malhi, A. Marcilla, J. Mariani, J. Mariscal, E. S. Martens-Uzunova, L. Martin-Jaular, M. C. Martinez, V. R. Martins, M. Mathieu, S. Mathivanan, M. Maugeri, L. K. McGinnis, M. J. McVey, D. G. Meckes Jr., K. L. Meehan, I. Mertens, V. R. Minciacchi, A. Möller, M. M. Jørgensen, A. Morales-Kastresana, J. Morhayim, F. Mullier, M. Muraca, L. Musante, V. Mussack, D. C. Muth, K. H. Myburgh, T. Najrana, M. Nawaz, I. Nazarenko, P. Nejsum, C. Neri, T. Neri, R. Nieuwland, L. Nimrichter, J. P. Nolan, E. N. Nolte-'t Hoen, N. N. Hooten, L. O'Driscoll, T. O'Grady, A. O'Loghlen, T. Ochiya, M. Olivier, A. Ortiz, L. A. Ortiz, X. Osteikoetxea, O. Østergaard, M. Ostrowski, J. Park, D. M. Pegtel, H. Peinado, F. Perut, M. W. Pfaffl, D. G. Phinney, B. C. Pieters, R. C. Pink, D. S. Pisetsky, E. P. von Strandmann, I. Polakovicova, I. K. Poon, B. H. Powell, I. Prada, L. Pulliam, P. Quesenberry, A. Radeghieri, R. L. Raffai, S. Raimondo, J. Rak, M. I. Ramirez, G. Raposo, M. S. Rayyan, N. Regev-Rudzki, F. L. Ricklefs, P. D. Robbins, D. D. Roberts, S. C. Rodrigues, E. Rohde, S. Rome, K. M. Rouschop, A. Rughetti, A. E. Russell, P. Saá, S. Sahoo, E. Salas-Huenuleo, C. Sánchez, J. A. Saugstad, M. J. Saul, R. M. Schiffelers, R. Schneider, T. H. Schøyen, A. Scott, E. Shahaj, S. Sharma, O. Shatnyeva, F. Shekari, G. V. Shelke, A. K. Shetty, K. Shiba, P. R.-M. Siljander, A. M. Silva, A. Skowronek, O. L. Snyder II, R. P. Soares, B. W. Sódar, C. Soekmadji, J. Sotillo, P. D. Stahl, W. Stoorvogel, S. L. Stott, E. F. Strasser, S. Swift, H. Tahara, M. Tewari, K. Timms, S. Tiwari, R. Tixeira, M. Tkach, W. S. Toh, R. Tomasini, A. C. Torrecilhas, J. P. Tosar, V. Toxavidis, L. Urbanelli, P. Vader, B. W. van Balkom, S. G. van der Grein, J. Van Deun, M. J. van Herwijnen, K. Van Keuren-Jensen, G. van Niel, M. E. van Royen, A. J. van Wijnen, M. H. Vasconcelos, I. J. Vechetti Jr., T. D. Veit, L. J. Vella, É. Velot, F. J. Verweij, B. Vestad, J. L. Viñas, T. Visnovitz, K. V. Vukman, J. Wahlgren, D. C. Watson, M. H. Wauben, A. Weaver, J. P. Webber, V. Weber, A. M. Wehman, D. J. Weiss, J. A. Welsh, S. Wendt, A. M. Wheelock, Z. Wiener, L. Witte, J. Wolfram, A. Xagorari, P. Xander, J. Xu, X. Yan, M. Yáñez-Mó, H. Yin, Y. Yuana, V. Zappulli, J. Zarubova, V. Žėkas, J.-Y. Zhang, Z. Zhao, L. Zheng, A. R. Zheutlin, A. M. Zickler, P. Zimmermann, A. M. Zivkovic, D. Zocco, E. K. Zuba-Surma, Minimal information for studies of extracellular vesicles 2018 (MISEV2018): A position statement of the International Society for Extracellular Vesicles and update of the MISEV2014 guidelines. *J. Extracell. Vesicles* **7**, 1535750 (2018).
53. T. Lener, M. Gimona, L. Aigner, V. Börger, E. Buzas, G. Camussi, N. Chaput, D. Chatterjee, F. A. Court, H. A. Del Portillo, L. O'Driscoll, S. Fais, J. M. Falcon-Perez, U. Felderhoff-Mueser, L. Fraile, Y. S. Gho, A. Görgens, R. C. Gupta, A. Hendrix, D. M. Hermann, A. F. Hill, F. Hochberg, P. A. Horn, D. de Kleijn, L. Kordelas, B. W. Kramer, E.-M. Krämer-Albers, S. Laner-Plamberger, S. Laitinen, T. Leonardi, M. J. Lorenowicz, S. K. Lim, J. Lötvall, C. A. Maguire, A. Marcilla, I. Nazarenko, T. Ochiya, T. Patel, S. Pedersen, G. Pocsfalvi, S. Pluchino, P. Quesenberry, I. G. Reischl, F. J. Rivera, R. Sanzenbacher, K. Schallmoser, I. Slaper-Cortenbach, D. Strunk, T. Tonn, P. Vader, B. W. M. van Balkom, M. Wauben,

S. E. Andaloussi, C. Théry, E. Rohde, B. Giebel, Applying extracellular vesicles based therapeutics in clinical trials – An ISEV position paper. *J. Extracell. Vesicles* **4**, 30087 (2015).
54. J. A. Welsh, D. C. I. Goberdhan, L. O'Driscoll, E. I. Buzas, C. Blenkiron, B. Bussolati, H. Cai, D. D. Vizio, T. A. P. Driedonks, U. Erdbrügger, J. M. Falcon-Perez, Q.-L. Fu, A. F. Hill, M. Lenassi, S. K. Lim, M. G. Mahoney, S. Mohanty, A. Möller, R. Nieuwland, T. Ochiya, S. Sahoo, A. C. Torrecilhas, L. Zheng, A. Zijlstra, S. Abuelreich, R. Bagabas, P. Bergese, E. M. Bridges, M. Brucale, D. Burger, R. P. Carney, E. Cocucci, R. Crescitelli, E. Hanser, A. L. Harris, N. J. Haughey, A. Hendrix, A. R. Ivanov, T. Jovanovic-Talisman, N. A. Kruh-Garcia, V. Ku'ulei-Lyn Faustino, D. Kyburz, C. Lässer, K. M. Lennon, J. Lötvall, A. L. Maddox, E. S. Martens-Uzunova, R. R. Mizenko, L. A. Newman, A. Ridolfi, E. Rohde, T. Rojalin, A. Rowland, A. Saftics, U. S. Sandau, J. A. Saugstad, F. Shekari, S. Swift, D. Ter-Ovanesyan, J. P. Tosar, Z. Useckaite, F. Valle, Z. Varga, E. van der Pol, M. J. C. van Herwijnen, M. H. M. Wauben, A. M. Wehman, S. Williams, A. Zendrini, A. J. Zimmerman, MISEV Consortium, C. Théry, K. W. Witwer, Minimal information for studies of extracellular vesicles (MISEV2023): From basic to advanced approaches. *J Extracell Vesicles* **13**, e12404 (2024).
55. F. Puhm, T. Afonyushkin, U. Resch, G. Obermayer, M. Rohde, T. Penz, M. Schuster, G. Wagner, A. F. Rendeiro, I. Melki, C. Kaun, J. Wojta, C. Bock, B. Jilma, N. Mackman, E. Boilard, C. J. Binder, Mitochondria are a subset of extracellular vesicles released by activated monocytes and induce type I IFN and TNF responses in endothelial cells. *Circ. Res.* **125**, 43–52 (2019).
56. S. Ma, X. Xing, H. Huang, X. Gao, X. Xu, J. Yang, C. Liao, X. Zhang, J. Liu, W. Tian, L. Liao, Skeletal muscle-derived extracellular vesicles transport glycolytic enzymes to mediate muscle-to-bone crosstalk. *Cell Metab.* **35**, 2028–2043.e7 (2023).
57. Y. Wang, P. Lou, Y. Xie, S. Liu, L. Li, C. Wang, D. Du, Y. Chen, Y. Lu, J. Cheng, J. Liu, Nutrient availability regulates the secretion and function of immune cell-derived extracellular vesicles through metabolic rewiring. *Sci. Adv.* **10**, eadj1290 (2024).
58. L. Zheng, Z. Rao, Y. Guo, P. Chen, W. Xiao, High-intensity interval training restores glycolipid metabolism and mitochondrial function in skeletal muscle of mice with Type 2 diabetes. *Front. Endocrinol. (Lausanne)* **11**, 561 (2020).

Acknowledgments: We thank X. Yang and X. Chen from the Animal Experimental Center of West China Hospital for assisting with the animal experiments, and S. Peng from the Core Facilities of West China Hospital for providing technical assistance with the confocal microscopy. **Funding:** This study was partly supported by the National Natural Science Foundation of China (grant 32271438 to J.L., grant 82472129 to J.L., and grant 32071453 to J.L.), Sichuan Science and Technology Program (grant 2024NSFSC0586 to J.L.), and 1.3.5 Project for Disciplines of Excellence (grant ZYYC23001 to J.L.), West China Hospital of Sichuan University. **Author contributions:** Conceptualization: J.L. and P.L. Methodology: P.L., X.Z., J.L., Y.X., Y.Z., and Y.W. Investigation: P.L., J.L., X.Z., and C.W. Resources: J.L. Funding acquisition: J.L. Data curation: P.L., X.Z., and J.L. Validation: P.L., X.Z., S.L., Y.L., Y.X., Y.Z., Y.W., and M.W. Formal analysis: P.L., X.Z., S.L., C.W., Y.L., and M.W. Supervision: J.L. Project administration: J.L. Visualization: P.L., X.Z., and J.L. Writing–original draft: P.L. and J.L. Writing–review and editing: P.L., J.L., X.Z., S.L., C.W., Y.L., Y.X., Y.Z., Y.W., and M.W. All experiments were conducted under the supervision of J.L. All authors contributed to the design development, data interpretation, and manuscript editing work. **Competing interests:** The authors declare that they have no competing interests. **Data and materials availability:** All data needed to evaluate the conclusions in the paper are present in the paper and/or the Supplementary Materials.

Submitted 12 September 2024
Accepted 6 June 2025
Published 16 July 2025
10.1126/sciadv.adt1318